

On the stability relations between tidal asymmetry and morphologies of tidal basins and estuaries

Zhou, Zeng; Coco, Giovanni; Townend, Ian; Gong, Zheng; Wang, Zhengbing ; Zhang, Changkuan

DOI

[10.1002/esp.4366](https://doi.org/10.1002/esp.4366)

Publication date

2018

Document Version

Accepted author manuscript

Published in

Earth Surface Processes and Landforms

Citation (APA)

Zhou, Z., Coco, G., Townend, I., Gong, Z., Wang, Z., & Zhang, C. (2018). On the stability relations between tidal asymmetry and morphologies of tidal basins and estuaries. *Earth Surface Processes and Landforms*, 43(9), 1943-1959. <https://doi.org/10.1002/esp.4366>

Important note

To cite this publication, please use the final published version (if applicable).
Please check the document version above.

Copyright

Other than for strictly personal use, it is not permitted to download, forward or distribute the text or part of it, without the consent of the author(s) and/or copyright holder(s), unless the work is under an open content license such as Creative Commons.

Takedown policy

Please contact us and provide details if you believe this document breaches copyrights.
We will remove access to the work immediately and investigate your claim.

On the stability relationships between tidal asymmetry and morphologies of tidal basins and estuaries

Zeng Zhou^{1,2}, Giovanni Coco², Ian Townend^{3,5}, Zheng Gong^{*1,5}, Zhengbing Wang⁴, and Changkuan Zhang⁵

¹Jiangsu Key Laboratory of Coast Ocean Resources Development and Environment Security, Hohai University, Nanjing, China

²School of Environment, University of Auckland, New Zealand

³Ocean and Earth Sciences, University of Southampton, UK

⁴Faculty of Civil Engineering and Geosciences, Delft University of Technology, Delft, Netherlands

⁵College of Harbour, Coastal and Offshore Engineering, Hohai University, Nanjing, China

Abstract

Simple stability relationships are practically useful to provide a rapid assessment of coastal and estuarine landforms in response to human interventions and long-term climate change. In this contribution, we review a variety of simple stability relationships which are based on the analysis of tidal asymmetry (shortened to “TA”). Most of the existing TA-based stability relationships are derived using the one-dimensional tidal flow equations assuming a certain regular shape of the tidal channel cross-sections. To facilitate analytical solutions, specific assumptions inevitably need to be made e.g. by linearising the friction term and dropping some negligible terms in the tidal flow equations. We find that three major types of TA-based stability relationships have been proposed between three non-dimensional channel geometric ratios (represented by the ratio of channel widths, ratio of wet surface areas and ratio of storage volumes) and the tide-related parameter a/h (i.e.

*Corresponding author. Email: gongzheng@hhu.edu.cn

24 the ratio between tidal amplitude and mean water depth). Based on established
25 geometric relations, we use these non-dimensional ratios to re-state the existing
26 relationships so that they are directly comparable. Available datasets are further
27 extended to examine the utility of these TA-based relationships. Although a cer-
28 tain agreement is shown for these relationships, we also observe a large scatter of
29 data points which are collected in different types of landscape, hydrodynamic and
30 sedimentologic settings over the world. We discuss in detail the potential reasons
31 for this large scatter and subsequently elaborate on the limited applicability of the
32 various TA-based stability relationships for practical use. We highlight the need to
33 delve further into what constitutes equilibrium and what is needed to develop more
34 robust measures to determine the morphological state of these systems.

35 **Keywords:** tidal basins, estuarine morphologies, tidal asymmetry, stability
36 relationships

37 **1 Introduction**

38 Tidal basins and estuaries are highly complex coastal systems that have evolved rapidly
39 during the Holocene transgression and have been shaped by various interactions be-
40 tween hydrodynamics, geomorphology, biological activities, climate variations and hu-
41 man interventions. Nonetheless, analyses of field observations indicate that the gross
42 characteristics of these complicated landscapes when they are morphologically sta-
43 ble (i.e. at or near to equilibrium) can be satisfactorily described by relationships that
44 are fairly simple (e.g. Jarrett, 1976; Friedrichs and Madsen, 1992; Gao and Collins,
45 1994; Dronkers, 1998; Wang et al., 1999; Whitehouse, 2006; Friedrichs, 2010; Tow-
46 nend, 2012; Dronkers, 2016; Zhou et al., 2017). These simple relationships prove to
47 be useful not only for indicating morphological equilibrium state, but more importantly
48 for providing clues on the response of tidal basins and estuaries to increasing human
49 activities, or accelerating sea level rise (Friedrichs et al., 1990; Dissanayake et al.,
50 2012; van der Wegen, 2013), as well as for assessing the resilience or adaptation time

51 of these vulnerable systems after human intervention (Wang et al., 2002; Dastgheib
52 et al., 2008).

53 Specifically, tidal asymmetry (hereafter indicated by “TA”), i.e. the inequality of flood
54 and ebb durations, has been widely used to derive such stability relationships and
55 adopted as an indicator for predicting the further evolution of tidal basin and estuary
56 morphologies. TA is generated by the distortion of tidal waves propagating on conti-
57 nental shelves and entering basins or estuaries, and is termed as flood dominance if
58 the flood duration is shorter (and flood velocity is larger) than the ebb, while the op-
59 posite condition is called ebb dominance. This has been extensively discussed in a
60 wide literature in terms of field observations, theoretical analyses and numerical mod-
61 elling because of its importance in producing the residual sediment transport which
62 in turn essentially determines the long-term morphological evolution of tidal systems
63 (see, e.g. Dronkers, 1986, 1998; Wang et al., 1999; Brown and Davies, 2010; Nidzieko
64 and Ralston, 2012).

65 From a hydrodynamic point of view, the distortion of tidal wave during propagation
66 can be represented as the non-linear growth of harmonics of the principal astronomical
67 constituents, particularly the semi-diurnal constituent M_2 and its first harmonic overtide
68 M_4 (Boon and Byrne, 1981; Aubrey and Speer, 1985). As an example, the distorted
69 tidal sea-surface (η) and velocity (u) may be approximated by a superposition of M_2
70 and M_4 as (Friedrichs and Aubrey, 1988):

$$\eta = a_{M_2} \cos(\omega t - \theta_{M_2}) + a_{M_4} \cos(2\omega t - \theta_{M_4}) \quad (1a)$$

$$u = U_{M_2} \cos(\omega t - \phi_{M_2}) + U_{M_4} \cos(2\omega t - \phi_{M_4}) \quad (1b)$$

71 where t is time, ω is the M_2 tidal frequency (and hence the M_4 tidal frequency is 2ω), a
72 is the tidal height amplitude, U is the tidal velocity amplitude, θ is the tidal height phase,
73 and ϕ is the tidal velocity phase.

74 The relative sea-surface phase difference of M_4 and M_2 ($\theta = 2\theta_{M_2} - \theta_{M_4}$) generally

75 indicates that a system is flood-dominated if $0 < \theta < \pi$ or ebb-dominated if $\pi < \theta < 2\pi$.
 76 Alternatively, the relative velocity phase difference of M_4 and M_2 ($\phi = 2\phi_{M_2} - \phi_{M_4}$) can
 77 also be used to indicate that a system is flood-dominated ($-\pi/2 < \phi < \pi/2$) or ebb-
 78 dominant ($\pi/2 < \phi < 3\pi/2$). The most significant flood-dominated and ebb-dominated
 79 conditions occur when the relative sea-surface phase differences (θ) are respectively
 80 $\pi/2$ and $3\pi/2$ (Figure 1a and c), or alternatively the relative velocity phase differences
 81 (ϕ) are respectively 0 and π (Figure 1b and d). The ratio of their amplitudes (a_{M_4}/a_{M_2} or
 82 U_{M_4}/U_{M_2}) suggests the significance of flood- or ebb-dominance. A number of studies
 83 have also highlighted the generation and characteristics of TA in areas that are subject
 84 to diurnal or mixed tidal regimes (Ranasinghe and Pattiaratchi, 2000; Nidziko, 2010;
 85 Jewell et al., 2012).

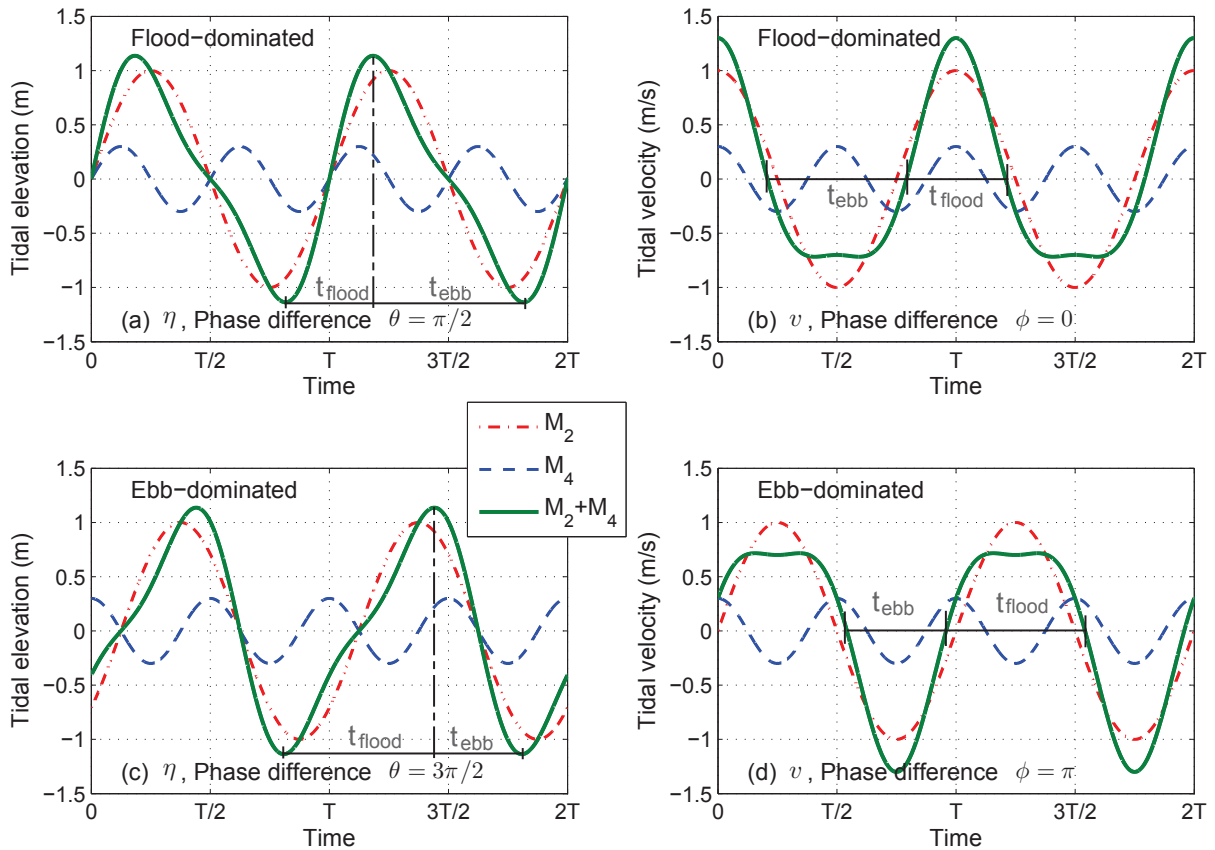


Figure 1: Examples of strongest tidal asymmetry conditions based on the superposition of the semi-diurnal constituent M_2 and its first harmonic overtide M_4 . The M_2 tidal period T of the horizontal axis is approximately 12.42 hours. Panels (a) and (b) show strongest flood dominance using relative sea-surface and velocity differences (with shorter flood durations t_{flood}), while similarly panels (c) and (d) show strongest ebb dominance (with shorter ebb durations t_{ebb}). This figure is plotted following Friedrichs and Aubrey (1988).

86 The distorted tidal wave is one of the key contributors for residual sediment trans-
87 port which generally occurs under two conditions (Dronkers, 1986): (1) unequal maxi-
88 mum flood and ebb velocities as the sediment transport responds non-linearly to veloc-
89 ities (mainly responsible for the transport of coarse sediment), and (2) unequal ebb and
90 flood slack water periods during which sediments fall and settle (mainly influences the
91 residual flux of fine sediment). Importantly, these two conditions can co-exist. Land-
92 ward residual sediment transport is usually associated with flood dominance resulting
93 in the infilling of tidal basins and estuaries, while seaward residual transport associated
94 with ebb dominance leads to the erosion of the system. As long as the residual sed-
95 iment transport exists, morphological changes will occur (Zhou et al., 2017). In other
96 words, a morphologically stable state can only be present when residual sediment
97 transport vanishes.

98 While TA has significant influence on the evolution of morphological features, the
99 opposite is also true: the geometric characteristics of tidal basins and estuaries to a
100 large extent determine the propagation of tidal waves, and hence promote the develop-
101 ment of TA. In fact, tidal landforms tend to evolve to an equilibrium state by developing a
102 morphology that offsets either flood dominance (resulting from, e.g. offshore TA or local
103 baroclinic effects) or ebb dominance (resulting from, e.g. compensation for Stokes drift
104 due to the phase lag between the times of high/low water and corresponding high/low
105 slack water, or seaward fluvial discharge). Previous studies show that an estuarine
106 system with large tidal flats tends to decrease flood tide duration and enhance the ef-
107 fects of channel friction, favouring flood dominance (Boon and Byrne, 1981; Aubrey and
108 Speer, 1985; Dronkers, 1986). Conversely, a system of relatively deep channels with
109 an absence of large intertidal flats generally promotes ebb dominance. Some studies
110 have confirmed that TA and its associated residual sediment transport are gradually
111 reduced when an evolving tidal system is approaching a morphologically stable state
112 (e.g. Lanzoni and Seminara, 2002; van der Wegen and Roelvink, 2008; van Maanen
113 et al., 2011; Guo et al., 2014). Recent studies based on numerical models also confirm

114 that morphological equilibrium requires that the system adjusts itself towards reducing
115 flood or ebb dominance (Dastgheib et al., 2008; Toffolon and Lanzoni, 2010; van der
116 Wegen, 2013; Zhou et al., 2014b). Therefore, TA acts as an important indicator for the
117 morphological state of a tidal system which may be in equilibrium (i.e. characterised
118 by a vanishing TA) or potentially importing/exporting sediment (i.e. characterised by
119 flood/ebb dominance).

120 In order to quantitatively describe the morphological state of tidal landforms, sim-
121 ple stability relationships between hydraulic parameters (e.g. tidal amplitude and wa-
122 ter depth) and geometric form parameters (e.g. tidal channel/flat width, wet surface
123 area and storage volume) have been developed based on either analytical or numeri-
124 cal studies. Though all the proposed stability relationships have been assessed in the
125 context of real systems, few of them have been examined using an extensive worldwide
126 dataset. Furthermore, none to our knowledge have been applied in conjunction with
127 other methods to establish whether TA is a necessary and sufficient condition to de-
128 termine equilibrium in these systems. Moreover, the applicability and the assumptions
129 of these relationships have not been well examined. For instance, some relationships
130 are derived based on a prismatic channel of constant width and depth, and hence their
131 applicability to convergent systems remains questionable.

132 With the above in mind, the objectives of this study include: (i) to thoroughly review
133 the existing theories and their associated stability relationships, clarifying their physical
134 background; (ii) to inter-compare those relationships by conversions of the main geo-
135 metric parameters (e.g. conversions between length, area and volume ratios); and (iii)
136 to discuss their validity and applicability in comparison with the measured datasets that
137 can be found in the literature. It must be stressed that this does not provide a validation
138 of the relationships. It simply shows how real systems compare. A validation would
139 require some independent measure of proximity to morphological stability and this is
140 beyond the scope of this paper.

2 Theories and existing formulations

The one-dimensional (1D) tidal flow equations describing the conservation of mass and momentum are often used to explore the TA-based stability relationships, and read:

$$B \frac{\partial \eta}{\partial t} + \frac{\partial A_c u}{\partial x} = 0 \quad (2a)$$

$$\underbrace{\frac{\partial u}{\partial t}}_{(i)} + \underbrace{u \frac{\partial u}{\partial x}}_{(ii)} + \underbrace{g \frac{\partial \eta}{\partial x}}_{(iii)} + \underbrace{\frac{c_d u |u|}{h}}_{(iv)} - \underbrace{\frac{\partial}{\partial x} \left(\nu \frac{\partial u}{\partial x} \right)}_{(v)} = 0 \quad (2b)$$

where B is the cross-sectional width at water surface, h is the water depth at mean sea level, $A_c = B_c h$ is the flow-carrying cross-sectional area (B_c is averaged channel width), x is the longitudinal coordinate with $x = 0$ at estuary mouth, c_d is the bed friction coefficient and ν is the turbulence viscosity coefficient. To describe a funnelling tidal system which is commonly observed in nature, an exponentially converging function of channel width is often assumed ($B_c = B_{mo} \exp(-x/L_b)$, where B_{mo} is the channel width at estuary mouth and L_b is the convergence length, see e.g. Davies and Woodroffe, 2010). For a non-convergent channel, the value of convergence length tends to be infinity (i.e. $L_b = \infty$).

The underlined terms (i)-(v) in the momentum equation (2b) physically represent, one by one, the contributions of local inertia, advective inertia, slope gradient, bottom friction, and horizontal diffusion. Non-dimensional scaling analyses indicate that the advective inertia term (ii) and horizontal diffusion term (v) are small compared to other terms in shallow tidal basins and estuaries (Parker, 1991; Friedrichs, 2010; Dronkers, 2016) and hence can be neglected.

With terms (ii) and (v) eliminated, analytical solution of Equation (2) is possible when the friction term (iv) is linearised ($c_d u |u|/h = r u/h$, where $r = 8c_d U/3\pi$, U is the tidal velocity magnitude) and the cross-section is schematised (Figure 2). This analytical solution has been extensively explored using various techniques (e.g. Dronkers,

163 1998; Friedrichs, 2010; van Rijn, 2011; Toffolon and Savenije, 2011; Cai et al., 2012;
 164 Savenije, 2012; Winterwerp and Wang, 2013; Dronkers, 2016). The details are not
 165 repeated here while the theoretical background and the implications for this study are
 166 briefly introduced in the following sections.

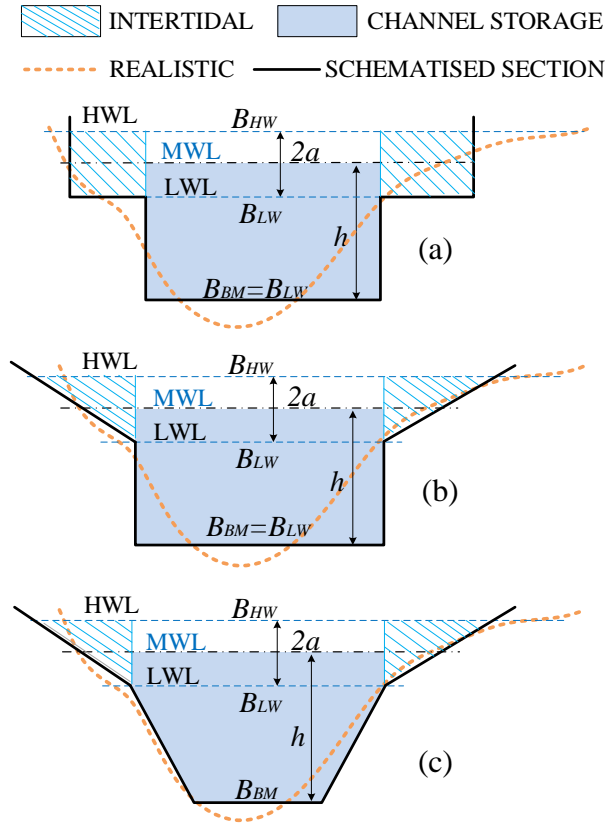


Figure 2: The schematic cross-sections adopted: (a) rectangular channel and flat used in Dronkers (1998), Winterwerp and Wang (2013), and Dronkers (2016), (b) rectangular channel and trapezoidal flat used in Friedrichs and Madsen (1992), (c) trapezoidal channel and flat used in Speer and Aubrey (1985), Friedrichs and Aubrey (1988), Friedrichs (2010) and Wang et al. (1999). B_{HW} , B_0 and B_{LW} are channel widths at high, mean and low water levels (HWL, MWL and LWL), B_{BM} is bottom channel width, a is tidal amplitude and h is mean channel depth.

167 2.1 Friedrichs-Aubrey-Speer's approach

168 Based on the pioneering work of Aubrey and Speer (1985) and Speer and Aubrey
 169 (1985), Friedrichs and Aubrey (1988) concluded that two key parameters that can
 170 be used to determine the condition of TA are a/h (ratio between offshore tidal amplitude and mean water depth - taken to be the average channel depth in real systems)
 171 and V_S/V_C (ratio between the volume of intertidal storage and channel storage). They
 172

173 solved Equation (2) numerically (all terms included except the horizontal diffusion) and
 174 considered 84 combinations of channel geometries by varying channel depth and width
 175 (with other parameters set the same, i.e. channel length = 7 km, $c_d = 0.01$, $a = 0.75$ m,
 176 $B_{LW} = 2B_{BM} = 120(h - a)$, see Figure 2c).

177 Model results suggested that the morphologies of short and flood-dominated sys-
 178 tems primarily change due to increased a/h whereas ebb-dominated systems primarily
 179 due to increased V_S/V_C . For small a/h (< 0.2), virtually all estuaries are ebb-dominant
 180 and for large a/h (> 0.3) all estuaries are flood-dominated while only when a/h is be-
 181 tween 0.2 and 0.3, the system can be either moderately flood- or ebb- dominated,
 182 indicating equilibrium should be achieved at this range, depending on the other param-
 183 eter V_S/V_C . Their findings are generally consistent with the measured data along the
 184 U.S. Atlantic Coast, and later studies have followed this theory to look at estuarine con-
 185 ditions (e.g. Wang et al., 2002; Dastgheib et al., 2008). The numerical model results
 186 are obtained under the following conditions: (1) non-convergent uniform trapezoidal
 187 cross-sections, and (2) short and shallow channels where friction dominates over iner-
 188 tia terms. Therefore, the numerically generated TA-based curve (see the red dashed
 189 line in Figure 3) should not be adopted as a universally valid indicator for all types of
 190 tidal basins and estuaries (e.g. convergent, long and deep tidal landforms).

191 Apart from the numerical curve introduced above, Friedrichs and Madsen (1992)
 192 and Friedrichs (2010) also developed several other stability relationships via analytical
 193 approaches. Based on perturbation analysis of the friction-dominated 1D tidal equa-
 194 tions retaining only terms (iii) and (iv) of Equation (2b), Friedrichs and Madsen (1992)
 195 derived an explicit relationship using the schematic channel cross-section (Figure 2b),
 196 which reads:

$$\gamma_2 = \frac{5a}{3h} - \frac{\Delta B}{B_0} \quad (3)$$

197 where B_{HW} , B_0 and B_{LW} are channel widths at high, mean and low water levels (m),
 198 respectively, $B_0 = 0.5(B_{HW} + B_{LW})$, $\Delta B = 0.5(B_{HW} - B_{LW})$ is the amplitude of change

199 in channel width during one tidal cycle (m), and γ_2 is the non-dimensional TA parameter,
 200 flood and ebb dominance occur when $\gamma_2 > 0$ and $\gamma_2 < 0$, respectively. Hence, the
 201 morphological equilibrium state can be obtained theoretically when $\gamma_2 = 0$, and the
 202 following relation should be satisfied:

$$\frac{\Delta B}{B_0} = \frac{B_{HW} - B_{LW}}{B_{HW} + B_{LW}} = \frac{5a}{3h} \quad (4)$$

203 More recently, Friedrichs (2010) performed a leading-term Taylor expansion for a
 204 linearised solution of tidal wave speed based on shallow non-convergent estuaries,
 205 giving an analytical relationship which slightly differs from Equation (3), and reads:

$$\gamma_6 = 2\frac{a}{h} - \frac{\Delta B}{B_0} \quad (5)$$

206 In order to directly compare this analytical solution with the former numerical curve
 207 in Friedrichs and Aubrey (1988), he converted $\Delta B/B_0$ to V_S/V_C based on the schematic
 208 cross-section in Figure 2b and another volume-type relationship was derived:

$$\frac{V_S}{V_C} = \frac{4\left(\frac{a}{h}\right)^2}{1 - 2\frac{a}{h}} \quad (6)$$

209 The comparison between Equation (6) and the numerical curve indicated that the
 210 analytical solution reasonably reproduces the fully non-linear results of Friedrichs and
 211 Aubrey (1988). The same analysis was also performed for shallow and funnel-shaped
 212 estuaries, indicating that the relations (Eqs. 5 and 6) also hold qualitatively.

213 **2.2 Dronkers' theory**

214 Based on the analytical solution of 1D tidal Equation (2b) retaining terms (i), (iii) and
 215 (iv), Dronkers (1998) also identified two key parameters S_{HW}/S_{LW} (ratio between the
 216 wet surface area at high and low water level) and H_{HW}/H_{LW} (or written as $(h+a)/(h-a)$,
 217 a), ratio between the average channel depth at high and low water level) to exam-

218 ine the TA conditions in the Dutch tidal basins. The schematic channel cross-section
 219 considered is shown in Figure 2a and the basin was assumed to be straight and longi-
 220 tudinally uniform. To facilitate a more in-depth understanding, the derivation is briefly
 221 introduced herein. Assuming that the solution to the simplified 1D tidal equation follows
 222 a harmonic function, the tidal elevation and velocity can be obtained:

$$\eta = \frac{1}{2} a_L \{ e^{-\mu(x-L)} \cos [k(L-x) - \omega t] + e^{\mu(x-L)} \cos [k(L-x) + \omega t] \} \quad (7a)$$

$$u = \frac{1}{2} \frac{a_L}{h} \frac{S}{S_c} \omega \{ e^{-\mu(x-L)} \cos [k(L-x) - \omega t - \varphi] - e^{\mu(x-L)} \cos [k(L-x) + \omega t + \varphi] \} \quad (7b)$$

with:

$$k = \sqrt{\frac{\omega^2}{2gh} \frac{S}{S_c}} \left[1 + \sqrt{1 + \left(\frac{r}{\omega h} \right)^2} \right] \quad (8a)$$

$$\mu = \sqrt{\frac{\omega^2}{2gh} \frac{S}{S_c}} \left[-1 + \sqrt{1 + \left(\frac{r}{\omega h} \right)^2} \right] \quad (8b)$$

$$a_L = \frac{a}{\sqrt{\cos^2(kL) \cosh^2(\mu L) + \sin^2(kL) \sinh^2(\mu L)}} \quad (8c)$$

$$\cos \varphi = \frac{k}{\sqrt{k^2 + \mu^2}} \quad (8d)$$

223 where ω is tidal frequency ($\omega = 2\pi/T$), a_L is tidal amplitude at landward boundary
 224 and L is the channel length (m), S and S_c are wet horizontal surface area and the wet
 225 horizontal channel surface area (m²), respectively.

226 The times of high water (HW, t_{HW}) and low water (LW, t_{LW}) can be obtained by
 227 setting $\partial\eta/\partial t = 0$, and the times of high water slack (HWS, t_{HWS}) and low water slack
 228 (LWS, t_{LWS}) can be obtained by setting $u = 0$. For short tidal systems, Dronkers (1998)
 229 found that the following expressions can approximately hold at the estuary mouth ($x =$
 230 0):

$$t_{HWS} - t_{HW} \approx \frac{L^2}{\omega} k_{HW} \mu_{HW} \quad (9a)$$

$$t_{LWS} - t_{LW} \approx \frac{L^2}{\omega} k_{LW} \mu_{LW} \quad (9b)$$

$$\text{with } k\mu = \frac{4}{3\pi} \frac{\omega c_d U}{gh^2} \frac{S}{S_c} \quad (9c)$$

231 Assuming a symmetrical tide at the estuary mouth (i.e. $t_{HW} - t_{LW} = \pi/\omega$), the flood
232 duration can be obtained:

$$\Delta t_{flood} = \frac{\pi}{\omega} + \frac{L^2}{\omega} (k_{HW} \mu_{HW} - k_{LW} \mu_{LW}) = \frac{\pi}{\omega} + \frac{4L^2 c_d}{3\pi g} \left(\frac{U_{HW}}{h_{HW}^2} \frac{S_{HW}}{S_{c,HW}} - \frac{U_{LW}}{h_{LW}^2} \frac{S_{LW}}{S_{c,LW}} \right) \quad (10)$$

233 The duration of flood and ebb is equal (i.e. $= \pi/\omega$, or $T/2$) if $k_{HW} \mu_{HW} - k_{LW} \mu_{LW}$ is
234 zero in Equation (10). To describe the asymmetrical condition, Dronkers (1998) defined
235 a TA index:

$$\gamma_3 = \frac{k_{LW} \mu_{LW}}{k_{HW} \mu_{HW}} = \frac{S_{LW}}{S_{HW}} \left(\frac{h+a}{h-a} \right)^2 \frac{S_{c,HW}}{S_{c,LW}} \frac{U_{LW}}{U_{HW}} \quad (11)$$

236 where S_{HW} and S_{LW} are wet horizontal surface areas at high water and low water
237 (m^2), respectively; $S_{c,HW}$ and $S_{c,LW}$ are the horizontal channel surface areas at high
238 water and low water (m^2), respectively. A larger γ indicates a shorter flood duration
239 and hence more flood-dominant characteristic.

240 For relatively deep channels, $S_{c,HW}$ and $S_{c,LW}$ can be assumed to be equal. How-
241 ever, for shallow basins with extensive flats, $S_{c,HW}/S_{c,LW}$ may be considerably larger
242 than 1.0. Based on a number of Dutch tidal basins, the maximum velocities during
243 HW and LW were assumed to have a similar magnitude ($U_{LW} \approx U_{HW}$), resulting in a
244 simplified formulation of Dronkers' TA index:

$$\gamma_3 = \frac{S_{LW}}{S_{HW}} \left(\frac{h+a}{h-a} \right)^2 \quad (12)$$

245 In theory, a tidal system is in a stable configuration (when flood and ebb durations
 246 are approximately equal) if γ_3 equates to one. The field data of Dutch basins, however,
 247 show that γ_3 is often greater than 1.0 and $\gamma_3 = 1.21$ generally provides a good fit. The
 248 reasons that γ_3 is not exactly 1.0 can be many fold: (1) the terms $S_{c,HW}/S_{c,LW}$ and
 249 U_{LW}/U_{HW} in Equation (11) may not be assumed to be 1.0 for some tidal basins; (2)
 250 approximations of the quantities S_{HW}/S_{LW} and H_{HW}/H_{LW} measured in the field may
 251 not be accurate; (3) some assumptions for the derivation may not hold for certain tidal
 252 systems (e.g. many natural estuaries are not prismatic); and (4) the tide arriving at the
 253 estuary mouth can be asymmetrical.

254 In recognition of these limitations, Dronkers (2016) recently reconstructed the TA
 255 relationships using ratios of channel widths (typically at the mouth) instead of wet sur-
 256 face areas. One of the key assumptions is that a cyclic tide exists and can be used to
 257 represent the average sediment transport characteristics within the system over a long
 258 period. During this cyclic tide, the net sediment transport (which is assumed to vary as
 259 a function of flow velocity to the fourth power) is zero. Dronkers (2016) considered both
 260 non-convergent (i.e. channel width is constant) and convergent systems (i.e. channel
 261 width decreases exponentially from the mouth). The width-type stability relationships,
 262 for which the details of derivation can be found in Dronkers (2016), was obtained:

$$\frac{B_{HW} - B_{LW}}{B_{HW} + B_{LW}} = \gamma_9 \frac{a}{h} \quad (13a)$$

$$\text{for non-convergent basins: } \gamma_9 = \frac{7}{6} + \frac{h}{4a} \frac{\Delta t_{FR}^{mouth}}{\Delta t_S} \quad (13b)$$

$$\text{for convergent basins: } \gamma_9 = \frac{2p_1}{p_2 + 1/4} = f(L_b, r, k, \omega, h, h_s) \quad (13c)$$

263 where Δt_{FR}^{mouth} is the difference in duration of falling and rising tide at the mouth, Δt_S
 264 is the time delay given by the average between $t_{HWS} - t_{HW}$ and $t_{LWS} - t_{LW}$, and
 265 $\Delta t_S \approx rl^2/(3ghh_s)$, h_s is the representative water depth taking into account tidal flat, p_1
 266 and p_2 are lumped parameters which can be expressed as functions of L_b, r, k, ω, h

267 and h_s (see Dronkers, 2016 for details).

268 Based on the analysis of field data, Dronkers (2016) found that the value of γ_9
269 generally falls in the range of 1.5 to 2.0 for the Dutch tidal basins. Depending on the
270 local condition of the continental shelf of tidal basins, the offshore tidal wave can be
271 already distorted and often with a shorter flood duration (i.e. $\Delta t_{FR}^{mouth} > 0$). Hence, the
272 value of γ_9 is mostly larger than 7/6. Dronkers (2005) concluded that γ_9 is close to 2.0
273 for many tidal basins in Northwest European coast where the continental shelf is wide
274 (tidal wave can be considerably distorted so Δt_{FR}^{mouth} is large), while γ_9 is close to 1.0 for
275 tidal systems along the US Atlantic coast and UK east coast where the shelf is narrow.
276 On the other hand, channel convergence can also affect the performance of TA-based
277 relationships (e.g. via the convergence length L_b). Overall, the recent relationships
278 (Equation 13) developed by Dronkers (2016) indicate that the value of TA index (γ_9)
279 is highly site-dependent, and hence data points collected in tidal systems of different
280 regions worldwide may show large scatter when a single relationship is used.

281 **2.3 Wang's approach**

282 Wang et al. (1999) built on the theories of Friedrichs and Aubrey (1988) and Dronkers
283 (1998) and derived a relationship between a/h and V_S/V_C based on a similar cross-
284 section geometry (assuming the channel bottom width $B_{BM} = 0.5B_{LW}$) as adopted by
285 Friedrichs and Aubrey (1988). Wang's derivation also assumed: (1) frictionless tidal
286 propagation ($c = \sqrt{gA/B}$, A and B are cross-sectional area and width) and (2) equiv-
287 alent hydraulic water depth A/B at high and low water (implicitly assumes equivalent
288 propagation speed at high and low water). The original derivation as presented in
289 Wang et al. (1999) contains a minor error and was corrected in van der Wegen and
290 Roelvink (2008) and has been applied as an indicator for equilibrium in a number of
291 recent publications (e.g. van der Wegen et al., 2008; Dissanayake et al., 2012; van der
292 Wegen, 2013). Under the assumptions of Wang et al. (1999), the following relation
293 holds:

$$\frac{A_{HW}}{A_{LW}} = \frac{B_{HW}}{B_{LW}} \quad (14)$$

294 where A_{HW} and A_{LW} are the cross-sectional areas at high and low water (m^2), respec-
 295 tively. Following Wang et al. (1999), the same cross-section (Figure 2c, and assume
 296 $B_{BM} = 0.5B_{LW}$) is considered, hence the intertidal and channel storage volumes can
 297 be expressed as:

$$V_S = 2a(B_{HW} - B_{LW})L/2 \quad (15a)$$

$$V_C = \left(\frac{1}{2}B_{LW} + B_{LW}\right)(h - a)L/2 + aB_{LW}L \quad (15b)$$

298 where L is the representative channel length. When the intertidal storage area is not
 299 considered as flow-carry part, the conveyance cross-sectional areas at LW and HW
 300 read:

$$A_{LW} = \left(\frac{1}{2}B_{LW} + B_{LW}\right)(h - a)/2, \quad (16a)$$

$$A_{HW} = \left(\frac{1}{2}B_{LW} + B_{LW}\right)(h - a)/2 + 2aB_{LW} \quad (16b)$$

301 However, if the intertidal storage area is considered as flow-carry part, the con-
 302 conveyance cross-sectional areas at LW and HW read:

$$A_{LW} = \left(\frac{1}{2}B_{LW} + B_{LW}\right)(h - a)/2, \quad (17a)$$

$$A_{HW} = \left(\frac{1}{2}B_{LW} + B_{LW}\right)(h - a)/2 + 2a(B_{LW} + B_{HW})/2 \quad (17b)$$

303 Combining Equations (14-15) with Equation (16), we obtain the original relationship
 304 by Wang et al. (1999) who did not consider the intertidal storage area as a flow-carrying

305 part:

$$\frac{A_{HW}}{A_{LW}} = 1 + \frac{8}{3} \frac{\frac{a}{h}}{1 - \frac{a}{h}} \quad (18a)$$

$$\frac{V_S}{V_C} = \frac{8}{3} \frac{\left(\frac{a}{h}\right)^2}{1 - \frac{a}{h}} \left(\frac{3}{4} + \frac{1}{4} \frac{a}{h}\right)^{-1} \quad (18b)$$

306 If the intertidal storage area is considered as a part that can carry flow (flow-
307 carrying), Equation (17) should be adopted instead of Equation (16), resulting in:

$$\frac{A_{HW}}{A_{LW}} = 1 + \frac{8}{3} \frac{\frac{a}{h}}{1 - \frac{7a}{3h}} \quad (19a)$$

$$\frac{V_S}{V_C} = \frac{8}{3} \frac{\left(\frac{a}{h}\right)^2}{1 - \frac{7a}{3h}} \left(\frac{3}{4} + \frac{1}{4} \frac{a}{h}\right)^{-1} \quad (19b)$$

308 The relationships represented by Equations (18) and (19) differ only because of the
309 different definitions of the conveyance section. Based on Equations (18b) and (19b), a
310 further consideration of the theory from Dronkers (1998) should result in the following
311 equations:

$$\frac{V_S}{V_C} = \frac{8}{3} \frac{\left(\frac{a}{h}\right)^2}{1 - \frac{a}{h}} \left(\frac{1 + \frac{a}{h}}{1 - \frac{a}{h}}\right) \left(\frac{3}{4} + \frac{1}{4} \frac{a}{h}\right)^{-1} \quad (20)$$

$$\frac{V_S}{V_C} = \frac{8}{3} \frac{\left(\frac{a}{h}\right)^2}{1 - \frac{7a}{3h}} \left(\frac{1 + \frac{a}{h}}{1 - \frac{a}{h}}\right) \left(\frac{3}{4} + \frac{1}{4} \frac{a}{h}\right)^{-1} \quad (21)$$

312 Compared with Equation (21), the minor difference in the derivation of Wang et al.
313 (1999), i.e. Equation (20), is the factor 7/3 in the expression because of the exclusion
314 of intertidal storage area as flow conveyance part. This will be further discussed in the

315 following sections.

316 **2.4 Overview of existing TA-based stability relationships**

317 To the authors' knowledge, all the existing TA-based stability formulations describing
318 the relationships between tidal morphologies and hydrodynamic parameters have been
319 summarised in Table 1, which are referred to as R1-R9 for simplicity. All relationships
320 were derived based on analytical methods except R1 which was numerically devel-
321 oped (Friedrichs and Aubrey, 1988). The formulation R8, linking S_{INT}/S_{HW} (the ratio
322 between surface intertidal area and surface HW area) with a/h , was developed by
323 van Maanen et al. (2013) for tidal network systems. Although this relationship was
324 proposed through numerical experiments, we later find that it can be easily derived an-
325 alytically by conversion from R3, and hence we categorise it as an analytical TA-based
326 relationship. The original relationship R4 developed by Wang et al. (1999) does not
327 include the intertidal storage area as flow-carrying, whereas R5 does.

328 Based on the considered geometric measure, these relationships can be generally
329 categorised as width-type (R2, R6 and R9), area-type (R3 and R8) and volume-type
330 (R1, R5 and R7). In the next sections, these three types of relationship are compared
331 by writing the equations in terms of common geometric quantities (i.e. width, area and
332 volume).

Table 1: List of existing TA-based stability relationships found in literature; refer to the text for the physical meaning of notations. Note: the relationship R5 (marked by ‘*’) is derived based on Wang et al. (1999), but differently, the intertidal storage area is considered to be flow-carrying.

Index	Source	TA-based stability relationship	Cross-section
R1	Friedrichs and Aubrey (1988)	Numerical curve between $\frac{V_S}{V_C}$ and $\frac{a}{h}$	Figure 2c
R2	Friedrichs and Madsen (1992)	$\gamma_2 = \frac{5a}{3h} - \frac{\Delta B}{B_0}$, where $\gamma_2 = 0$	Figure 2b
R3	Dronkers (1998)	$\gamma_3 = \left(\frac{H_{HW}}{H_{LW}}\right)^2 \frac{S_{LW}}{S_{HW}}$, γ_3 is site-dependent	Figure 2a
R4	Wang et al. (1999)	$\frac{V_S}{V_C} = \frac{8}{3} \frac{\left(\frac{a}{h}\right)^2}{1 - \frac{a}{h}} \left(\frac{1 + \frac{a}{h}}{1 - \frac{a}{h}}\right) \left(\frac{3}{4} + \frac{1}{4} \frac{a}{h}\right)^{-1}$	Figure 2c
R5*	This study	$\frac{V_S}{V_C} = \frac{8}{3} \frac{\left(\frac{a}{h}\right)^2}{1 - \frac{7a}{3h}} \left(\frac{1 + \frac{a}{h}}{1 - \frac{a}{h}}\right) \left(\frac{3}{4} + \frac{1}{4} \frac{a}{h}\right)^{-1}$	Figure 2c
R6	Friedrichs (2010)	$\gamma_6 = 2\frac{a}{h} - \frac{\Delta B}{B_0}$, where $\gamma_6 = 0$	Figure 2b
R7	Friedrichs (2010)	$\frac{V_S}{V_C} = \frac{4\left(\frac{a}{h}\right)^2}{1 - 2\frac{a}{h}}$	Figure 2b
R8	van Maanen et al. (2013)	$\frac{S_{INT}}{S_{HW}} = \frac{a}{h}$	Figure 2a
R9	Dronkers (2016)	$\frac{B_{HW} - B_{LW}}{B_{HW} + B_{LW}} = \gamma_9 \frac{a}{h}$, γ_9 is site-dependent	Figure 2a

3 Conversion and comparison

333

334 In the previous sections, we have reviewed the existing stability relationships that were
335 derived based on TA analyses (Table 1). In order to gain more insight into these rela-
336 tionships, it is useful to compare their differences and similarities. However, this is not
337 very straight-forward because different geometries were used to formulate these rela-
338 tionships. On the other hand, most of these relationships were only assessed against
339 limited and specific measured datasets at a regional scale. For instance, the area-
340 type relationship R3 developed by Dronkers (1998) was only examined for data of the
341 Dutch tidal basins, and similarly the volume-type relationship R1 was only compared
342 with the US data (Friedrichs and Aubrey, 1988). Therefore, it remains unclear how well

343 these relationships work at the global scale and their applicabilities need to be better
 344 examined.

345 In this section, we present the conversions among different geometric ratios (i.e.
 346 V_S/V_C , S_{HW}/S_{LW} , S_{INT}/S_{SW} , and $\Delta B/B_0$) according to corresponding theoretically
 347 based schematic cross-sections (Figure 2). By doing this, different TA-based relation-
 348 ships can be compared directly.

349 **3.1 Geometric conversion and datasets**

350 The conversion should be conducted based on the cross-section adopted. For all
 351 cross-sections considered in Figure 2, the following relations on channel widths, wet
 352 surface areas and water depths hold to first order:

$$S_{HW} = B_{HW}L, S_{LW} = B_{LW}L \quad (22a)$$

$$S_{INT} = S_{HW} - S_{LW} \quad (22b)$$

$$H_{HW} = h + a, H_{LW} = h - a \quad (22c)$$

353 The major difference regarding the conversion among these three types of cross-
 354 sections is in the expressions for channel and storage volumes:

$$V_S = 2a(S_{HW} - S_{LW}), V_C = hS_{LW} \text{ (Figure 2a)} \quad (23a)$$

$$V_S = 2aL\Delta B, \Delta B = (B_{HW} - B_{LW})/2, V_C = hLB_{LW} \text{ (Figure 2b)} \quad (23b)$$

$$V_S = 2aL\Delta B, V_C = (B_{LW}/2 + B_{LW})(h - a)L/2 + aB_{LW}L \text{ (Figure 2c)} \quad (23c)$$

355 Using Equations (22) and (23), datasets of different geometric ratios can be inter-
 356 converted, resulting in additional metrics for comparison (see Tables 2, 3 and 4 in
 357 the main text, and Table A1 in the appendix). Overall, four published datasets are

358 considered in this study: (a) the Dutch area-type data (S_{HW}/S_{LW}) provided in Dronkers
 359 (1998), (b) the US volume-type data (V_S/V_C) in Friedrichs and Aubrey (1988), (c) the
 360 UK data in terms of both area and volume (S_{HW}/S_{LW} and V_S/V_C) in Townend (2005),
 361 and (d) the width-type data (B_{HW}/B_{LW}) collected in a few countries and provided in
 362 Dronkers (2016).

363 For the US data, as pointed out by Friedrichs and Aubrey (1988), the magnitude of
 364 the ratio a/h alone may indicate the overall TA condition in shallow estuaries of the US
 365 Atlantic coast. They found that only tidal basins with a/h falling in the range of 0.2-0.3
 366 were close to equilibrium, hence only these locations in the US data are considered
 367 here for comparison. At the same time, it is worth noting that most of the relationships
 368 are derived based on the assumption that a/h is small. Therefore, from the UK dataset
 369 provided in Townend (2005), we only selected the tidal landforms with a value of a/h
 370 smaller than 0.5.

Table 2: Geometric parameters of the Dutch tidal basins. The left two ratios, S_{HW}/S_{LW} and H_{HW}/H_{LW} , are obtained from Dronkers (1998), and the rest are derived based on Equations (22) and (23a).

Data location	$\frac{S_{HW}}{S_{LW}}$	$\frac{H_{HW}}{H_{LW}}$	$\frac{a}{h}$	$\frac{V_S}{V_C}$	$\frac{S_{INT}}{S_{HW}}$	$\frac{B_{HW} - B_{LW}}{B_{HW} + B_{LW}}$
Western Scheldt	1.526	1.379	0.159	0.168	0.345	0.208
Eastern Scheldt	1.596	1.412	0.171	0.204	0.374	0.230
Texel Inlet	1.203	1.410	0.170	0.069	0.169	0.092
Eijerland Inlet	3.000	1.905	0.311	1.246	0.667	0.500
Vlie Inlet	1.688	1.644	0.244	0.335	0.407	0.256
Ameland Inlet	2.400	1.868	0.303	0.847	0.583	0.412
Pinkegat	4.462	3.000	0.500	3.462	0.776	0.634
Frysian Inlet	3.698	1.742	0.271	1.460	0.730	0.574
Lauwers Inlet	3.585	2.070	0.348	1.802	0.721	0.564
Ems-Dollard	1.810	1.56	0.219	0.355	0.448	0.288

Table 3: Geometric parameters of the US tidal basins for which the value of a/h is close to the range of 0.2-0.3. The left two ratios, a/h and V_S/V_C , are obtained from Friedrichs and Aubrey (1988), and the rest are derived based on Equations (22) and (23c).

Data location	$\frac{a}{h}$	$\frac{V_S}{V_C}$	$\frac{H_{HW}}{H_{LW}}$	$\frac{S_{HW}}{S_{LW}}$	$\frac{S_{INT}}{S_{HW}}$	$\frac{B_{HW} - B_{LW}}{B_{HW} + B_{LW}}$
Absecon, NJ	0.19	0.79	1.469	4.316	0.768	0.624
Strathmere, NJ	0.24	0.94	1.632	4.173	0.760	0.613
Townsend, NJ	0.25	1.14	1.667	4.653	0.785	0.646
Northam, VA	0.31	0.85	1.899	3.269	0.694	0.532
Little River, SC	0.25	0.73	1.667	3.373	0.703	0.543
North Inlet, SC	0.30	1.01	1.857	3.778	0.735	0.581
Price, SC	0.21	1.08	1.532	5.127	0.721	0.674
Capers, SC	0.22	0.68	1.564	3.488	0.611	0.554
Breach, SC	0.22	1.47	1.564	6.379	0.769	0.729
Folly, SC	0.21	0.88	1.532	4.363	0.676	0.627
Duplin, GA	0.21	0.91	1.532	4.478	0.684	0.635

Table 4: Geometric parameters of selected UK tidal basins and estuaries for which the value of a/h is smaller than 0.5. The left three ratios, a/h , V_S/V_C and S_{HW}/S_{LW} , are obtained from Townend (2005), and the rest are derived based on Equations (22) and (23c).

Data location	$\frac{a}{h}$	$\frac{V_S}{V_C}$	$\frac{S_{HW}}{S_{LW}}$	$\frac{H_{HW}}{H_{LW}}$	$\frac{S_{INT}}{S_{HW}}$	$\frac{B_{HW} - B_{LW}}{B_{HW} + B_{LW}}$
Teifi Estuary	0.223	0.038	1.703	1.573	0.413	0.260
Traeth Coch	0.229	0.170	2.470	1.593	0.595	0.424
Cromarty Firth	0.286	0.044	1.372	1.799	0.271	0.157
Firth of Tay	0.506	0.802	2.807	3.046	0.644	0.475
Firth of Forth	0.110	0.011	1.197	1.248	0.165	0.090
Tynninghame Bay	0.123	0.061	2.560	1.281	0.609	0.438
Blyth Estuary	0.197	0.875	6.295	1.491	0.841	0.726
Tyne Estuary	0.414	0.233	2.555	2.415	0.609	0.437
Tees Estuary	0.236	0.693	12.937	1.618	0.923	0.857
Ore-Alde-Butley	0.464	0.643	3.925	2.730	0.745	0.594
Thames Estuary	0.435	0.210	3.085	2.542	0.676	0.510
Medway Estuary	0.416	0.554	3.490	2.426	0.713	0.555
Portsmouth Harbour	0.494	0.179	2.155	2.951	0.536	0.366
Southampton Water	0.400	0.230	3.144	2.332	0.682	0.517
Newtown Estuary	0.374	0.209	1.963	2.197	0.491	0.325
Poole Harbour	0.396	0.207	1.613	2.314	0.380	0.235
The Fleet	0.453	0.569	3.802	2.655	0.722	0.584
Dart Estuary	0.387	0.173	1.776	2.261	0.437	0.279
Plymouth Sound	0.359	0.212	3.594	2.122	0.722	0.565
Falmouth	0.374	0.061	1.654	2.193	0.395	0.246
Helford Estuary	0.486	0.184	2.602	2.892	0.616	0.445

3.2 Volume-type relationships and comparison

The width-type relationships (R2 and R6 in Table 1) can be easily converted to volume-type using Equations (22) and (23). Based on the schematic cross-section (Figure 2b), Friedrichs (2010) converted R6 from width-type to volume-type relationship R7 to compare with a previous numerical result (Friedrichs and Aubrey, 1988). The relationship R2 can also be converted following Friedrichs (2010) using Equations (22) and (23b), resulting in another volume-type relationship:

$$\frac{V_S}{V_C} = \frac{\frac{10}{3} \left(\frac{a}{h}\right)^2}{1 - \frac{5a}{3h}} \quad (24)$$

Similarly, the width-type relationship R9 derived by Dronkers (2016) can also be converted to volume-type equation following the same method. However, the cross-section as shown in Figure 2a should be used for consistency. Using Equations (22) and (23a) and we obtain:

$$\frac{V_S}{V_C} = \frac{4\gamma_9 \left(\frac{a}{h}\right)^2}{1 - \gamma_9 \left(\frac{a}{h}\right)} \quad (25)$$

where γ_9 is the TA index between 1.0 and 2.0, depending on local condition of tidal landforms.

The area-type relationship described by R3 (Table 1) can also be converted to volume-type by adopting the simplified cross-section (Figure 2a) as assumed by Dronkers (1998, 2016), reads:

$$\frac{V_S}{V_C} = 2\frac{a}{h} \left[\frac{1}{\gamma_3} \left(\frac{1 + \frac{a}{h}}{1 - \frac{a}{h}} \right)^2 - 1 \right] \quad (26)$$

Assuming $\gamma_3 = 1$, i.e. theoretical equilibrium condition discussed before, Equation (26) can be simplified to:

$$\frac{V_S}{V_C} = \frac{8 \left(\frac{a}{h}\right)^2}{\left(1 - \frac{a}{h}\right)^2} \quad (27)$$

389 These volume-type relationships share some similarities in form and their compari-
 390 son with datasets is shown in Figure 3. Except the numerical curve R1, all relationships
 391 are analytical and generally display a similar trend. With the increase of V_S/V_C , a tidal
 392 system becomes more ebb-dominated, while it becomes more flood-dominated in case
 393 of an increasing a/h . Most of the relationships are visually clustered within the range in-
 394 dicated by the two lines described by Equation (21) with different TA indices ($\gamma_9 = 1, 2$).
 395 According to (Dronkers, 2016), the value of γ_9 should be theoretically larger than 1.0
 396 if the offshore tide is symmetrical. Therefore, it is reasonable to observe that other
 397 curves based on different approaches are all below the top dashed line (indicated by
 398 “Eq.21: $\gamma_9=1$ ”).

399 The datasets from three different countries show considerable scatter. The UK
 400 data exhibit a large relative tidal amplitude (a/h) and a small relative intertidal storage
 401 (V_S/V_C), so it appears that most of the selected UK estuaries are flood-dominated.
 402 Although with a small relative tidal amplitude ($0.2 < a/h < 0.3$), the selected US tidal
 403 basins are largely ebb-dominated because of the relatively large intertidal storage.
 404 Differently, the Dutch data points mostly lie within the cluster of curves, indicating that
 405 many of these tidal systems could be considered to be close to equilibrium based on
 406 the theoretical arguments used. The converted curve with a TA index $\gamma_3 = 1.21$ appears
 407 to provide a better fit with the Dutch data than $\gamma_3 = 1$, which is consistent with Dronkers
 408 (1998). The value of relative tidal amplitude a/h for most of the Dutch basins in this
 409 dataset is close to the range of 0.2 to 0.3, which according to Friedrichs and Aubrey
 410 (1988) is close to equilibrium. Therefore, though developed via different approaches,
 411 the theoretical indications out of Dronkers (1998) and Friedrichs and Aubrey (1988)
 412 share some similar characteristics.

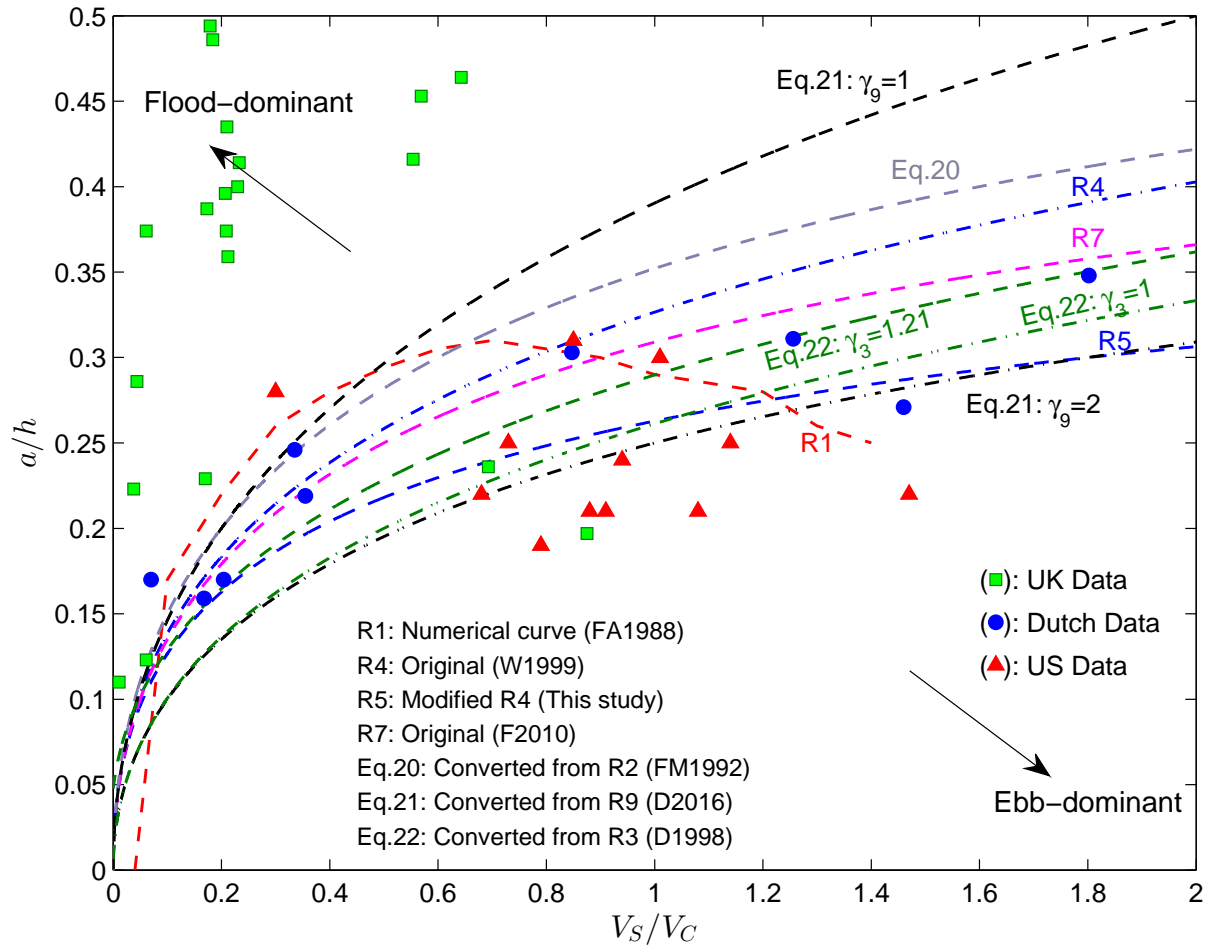


Figure 3: The existing and extended volume-type relationships between V_s/V_C and a/h as shown in Table 1 and derived in the main text. The points indicated by blue circles are the converted Dutch data from Dronkers (1998), red triangles are the original US data from Friedrichs and Aubrey (1988) and green squares are the original UK data from Townend (2005). Note the citations are shortened in the figure for simplicity (i.e. ‘FA1988’ = Friedrichs and Aubrey, 1988; ‘F2010’ = Friedrichs, 2010; ‘W1999’ = Wang et al., 1999; ‘FM1992’ = Friedrichs and Madsen, 1992; ‘D1998’ = Dronkers, 1998; ‘D2016’ = Dronkers, 2016) and this also holds for the following figures hereafter.

413 3.3 Area-type relationships and comparison

414 The volume-type relationship R5 can also be converted to area-type based on the
 415 trapezoidal cross-section (Figure 2c) following Wang et al. (1999). Using Equations
 416 (22) and (23c), we obtain:

$$\frac{S_{HW}}{S_{LW}} = 1 + \frac{8}{3} \frac{\left(\frac{a}{h}\right)}{1 - \frac{7a}{3h}} = \frac{1 + 2\frac{H_{HW}}{H_{LW}}}{5 - 2\frac{H_{HW}}{H_{LW}}} \quad (28)$$

417 The width-type relationships R2, R6 and R9 in fact share the same mathematical
 418 form because the expressions $\Delta B/B_0$ and $(B_{HW} - B_{LW})/(B_{HW} + B_{LW})$ are equal.
 419 Taking R9 as an example, it can be easily transformed to area-type (using $S_{HW} =$
 420 $B_{HW}L$ and $S_{LW} = B_{LW}L$):

$$\frac{S_{HW}}{S_{LW}} = \frac{(1 + \gamma_9)\frac{H_{HW}}{H_{LW}} + (1 - \gamma_9)}{(1 - \gamma_9)\frac{H_{HW}}{H_{LW}} + (1 + \gamma_9)} \quad (29)$$

421 where γ_9 is equal to 5/3 and 2 for the conversion of R2 and R6, respectively.

422 The above-discussed area-type relationships in terms of S_{HW}/S_{LW} are compared
 423 in Figure 4. Except the curve indicated by “Eq.25: $\gamma_9=1$ ”, all other relationships are
 424 relatively close in position and cluster within a narrow area. Comparable to the volume-
 425 type relationships, the horizontal axis S_{HW}/S_{LW} represents the capacity of intertidal
 426 storage and a larger S_{HW}/S_{LW} indicates a more ebb-dominated characteristic. The
 427 vertical axis H_{HW}/H_{LW} is somehow comparable to the relative tidal amplitude a/h
 428 and its increase indicates a more flood-dominated characteristic. They both reflect the
 429 potential for different propagation speeds at high and low water, which is the underlying
 430 cause of tidal asymmetry.

431 Similarly to Figure 3, the datasets of three different countries also show great scatter
 432 in the area-type plot (Figure 4), indicating the inherent consistency of these geometric
 433 ratios. The selected UK tidal landforms tend to be flood-dominated, while the US ones
 434 are mostly ebb-dominated. The Dutch tidal basins are generally close to equilibrium
 435 state, with points distributing around the curve R3 when $\gamma_3 = 1.21$. This is consistent
 436 with Dronkers (1998).

437 Many square points representing the UK estuaries appear to distribute around the
 438 converted equilibrium curve indicated by “Eq.25: $\gamma_9=1$ ” and away from the cluster of

439 curves. The US estuaries tend to fall below the cluster of curves. Whilst this may
 440 say something about relative TA in these systems, the results are not providing a clear
 441 indication of relative stability.

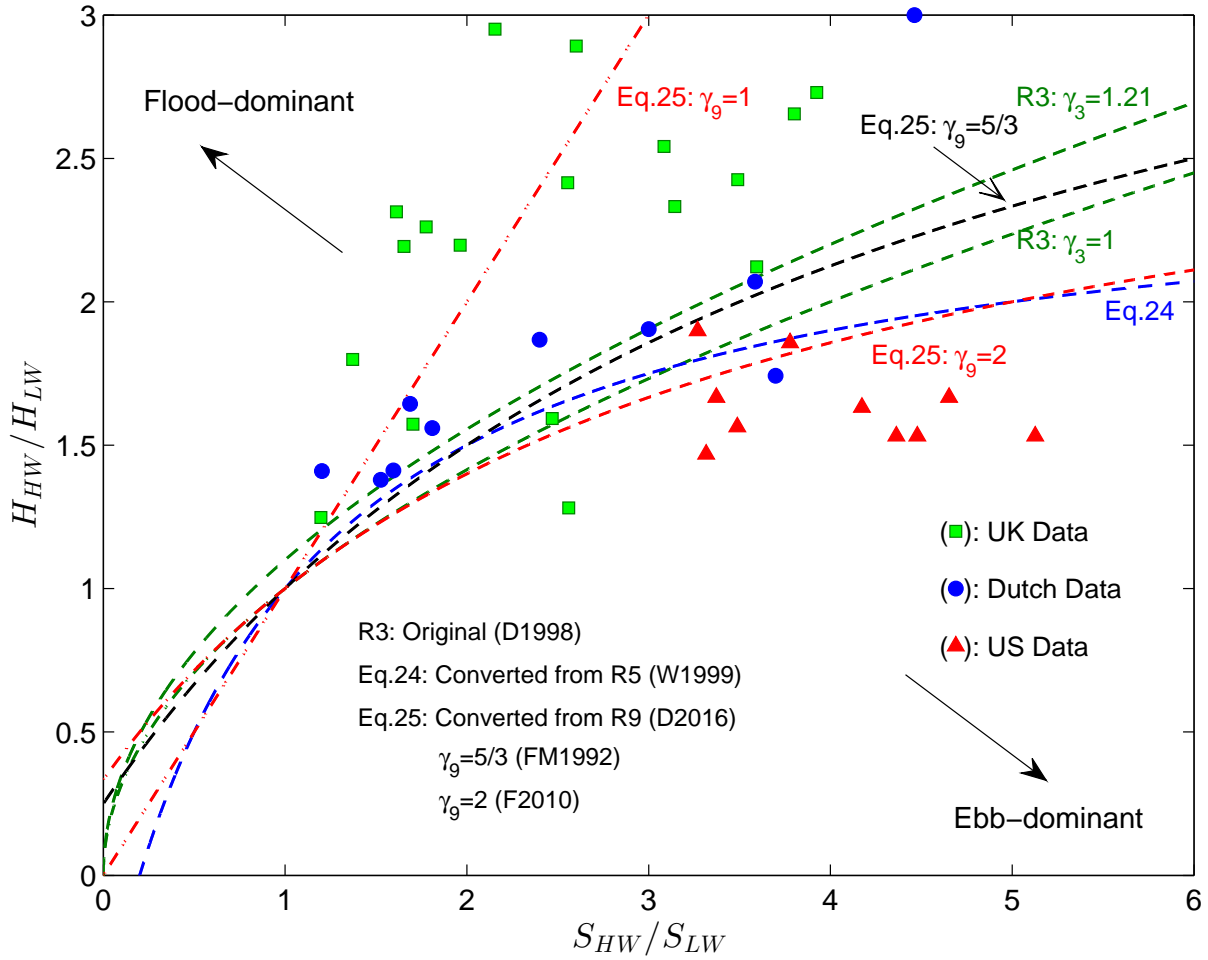


Figure 4: The existing and extended area-type relationships between S_{HW}/S_{LW} and H_{HW}/H_{LW} as shown in Table 1 and derived in the main text. The points indicated by blue circles are the original Dutch data from Dronkers (1998), red triangles are the converted US data from Friedrichs and Aubrey (1988) and green squares are the original UK data from Townsend (2005).

442 Based on the theory of Dronkers (2005), van Maanen et al. (2013) further defined a
 443 “relative intertidal area” as the ratio between surface intertidal area (S_{INT}) and the total
 444 surface area inundated at high tide (S_{HW}), see R8 in Table 1. Though lacking a rigorous
 445 mathematical proof, the result of their numerical experiments for reproducing long-term
 446 evolution of tidal networks agreed quite well with the linear area-type relationship R8.
 447 Here we present a short derivation which may explain why the relationship R8 works

448 for shallow tidal network systems. Recalling relationship R3 from Dronkers (1998) , we
449 assume $S_{INT} = S_{HW} - S_{LW}$ as a first approximation and hence:

$$\frac{S_{INT}}{S_{HW}} = 1 - \frac{S_{LW}}{S_{HW}} = (1 - \gamma_3^2) + \frac{\gamma_3^2}{\left(\frac{1 + a/h}{2}\right)^2} \frac{a}{h} \quad (30)$$

450 For the models considered in van Maanen et al. (2013), γ_3 is 1.0 when the theo-
451 retical equilibrium condition is reached, hence the first term at the right hand side of
452 the equation becomes zero and the second term can be simplified to a/h for shallow
453 tidal network systems (a and h can be close where tidal flats are present). Therefore,
454 Equation (30) can be simplified to relationship R8 which may be used as a first-order
455 indicator for shallow tidal network systems.

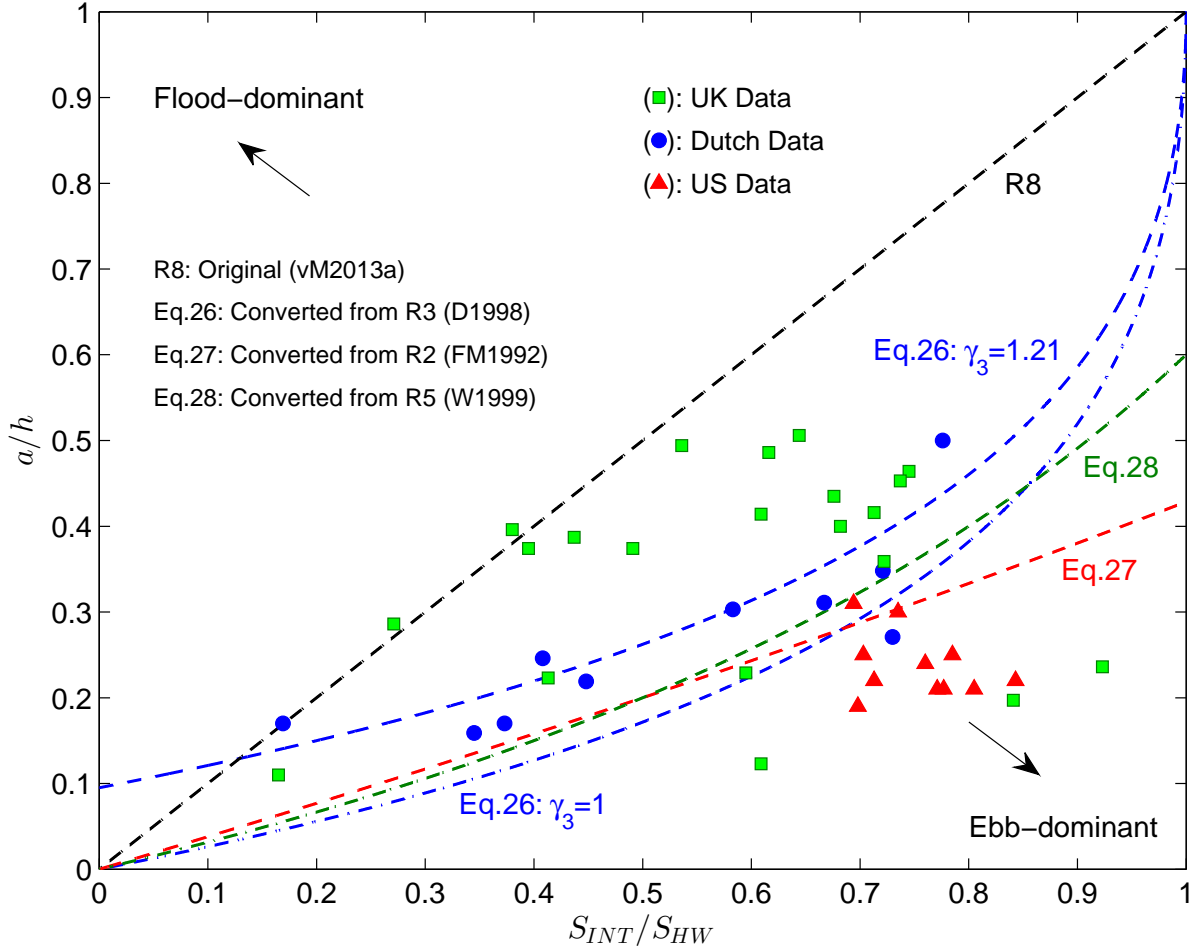


Figure 5: The existing and extended area-type relationships between S_{INT}/S_{HW} and a/h as shown in Table 1 and derived in the main text. The points indicated by blue circles are the original Dutch data from Dronkers (1998), red triangles are the converted US data from Friedrichs and Aubrey (1988) and green squares are the original UK data from Townend (2005). The shortened citation ‘vM2013a’ indicates van Maanen et al. (2013).

456 It is also interesting to rewrite the relationships developed by Friedrichs and Madsen
 457 (1992) and Wang et al. (1999) using S_{INT}/S_{HW} since this would provide a more direct
 458 indication for a tidal system with extensive tidal flats. We recall relationship R2 and use
 459 Equation (22), resulting in:

$$\frac{S_{INT}}{S_{HW}} = 2 \left(1 - \frac{1}{1 + \frac{5a}{3h}} \right) \quad (31)$$

460 Similarly, the relationship proposed by Wang et al. (1999) can also be easily con-
 461 verted to area-type (S_{INT}/S_{HW}) by using Equation (28):

$$\frac{S_{INT}}{S_{HW}} = 8 \left(1 - \frac{1}{1 + \frac{1}{3} \frac{a}{h}} \right) \quad (32)$$

462 A comparison of these S_{INT}/S_{HW} area-type relationships is shown in Figure 5.
 463 Since S_{INT}/S_{HW} is converted directly from S_{LW}/S_{HW} , the overall performance of these
 464 relationships are comparable to Figure 4. The converted relationship from R3 in Dronkers
 465 (1998), indicated here by Eq.26, shows a better agreement with the Dutch dataset
 466 when γ_3 is 1.21. Similarly with previous figures, the UK data points lie mostly in the
 467 flood-dominated zone while the US data are mainly located in the ebb-dominated zone.

468 It is noted that the numerically inferred linear relationship R8 by van Maanen et al.
 469 (2013) is located far from the cluster of other TA-based curves. Visually, all tidal
 470 landforms from three different countries can be categorised as ebb-dominated using
 471 R8, which is inconsistent with other theories and previously published findings (e.g.
 472 Friedrichs and Aubrey, 1988; Dronkers, 1998; Townend, 2005). However, R8 appears
 473 to define an upper flood-dominant bound of these TA-based relationships. The amount
 474 of intertidal area increases as tidal range increases, which appears to hold even for
 475 systems that are almost all intertidal. For these systems, the tidal distortion between
 476 high and low water tends to be large and favors flood-dominance. Although R8 ap-
 477 pears to work well with numerically produced tidal network systems, its applicability to
 478 natural tidal basins and estuaries merits further research.

479 **3.4 Width-type relationships and comparison**

480 Recently, Dronkers (2016) reformulated the TA-based relationships using widths in-
 481 stead of surface areas. The essence of the two types of TA-based stability relation-
 482 ships is the same, so Dronkers (2016) defined the ratio $(B_{HW} - B_{LW})/(B_{HW} + B_{LW})$
 483 as relative intertidal area. In fact, one may convert the original area-type relationship
 484 R3 developed by Dronkers (1998) to width-type using Equation (22), and this reads:

$$\frac{B_{HW} - B_{LW}}{B_{HW} + B_{LW}} = \frac{\left(1 + \frac{a}{h}\right)^2 - \gamma_3 \left(1 - \frac{a}{h}\right)^2}{\left(1 + \frac{a}{h}\right)^2 + \gamma_3 \left(1 - \frac{a}{h}\right)^2} \quad (33)$$

485 when γ_3 is 1.0, as assumed in several studies, the above expression becomes:

$$\frac{B_{HW} - B_{LW}}{B_{HW} + B_{LW}} = \frac{2\frac{a}{h}}{1 + \left(\frac{a}{h}\right)^2} \approx 2\frac{a}{h} \quad (34)$$

486 One can immediately notice that the above simplified relationship (assuming a/h
 487 is small) converted from Dronkers' area-type relationship R3 shares a consistent form
 488 with the recently-developed R9. Noticeably, it also coincides with the width-type rela-
 489 tionship R6 developed by Friedrichs (2010).

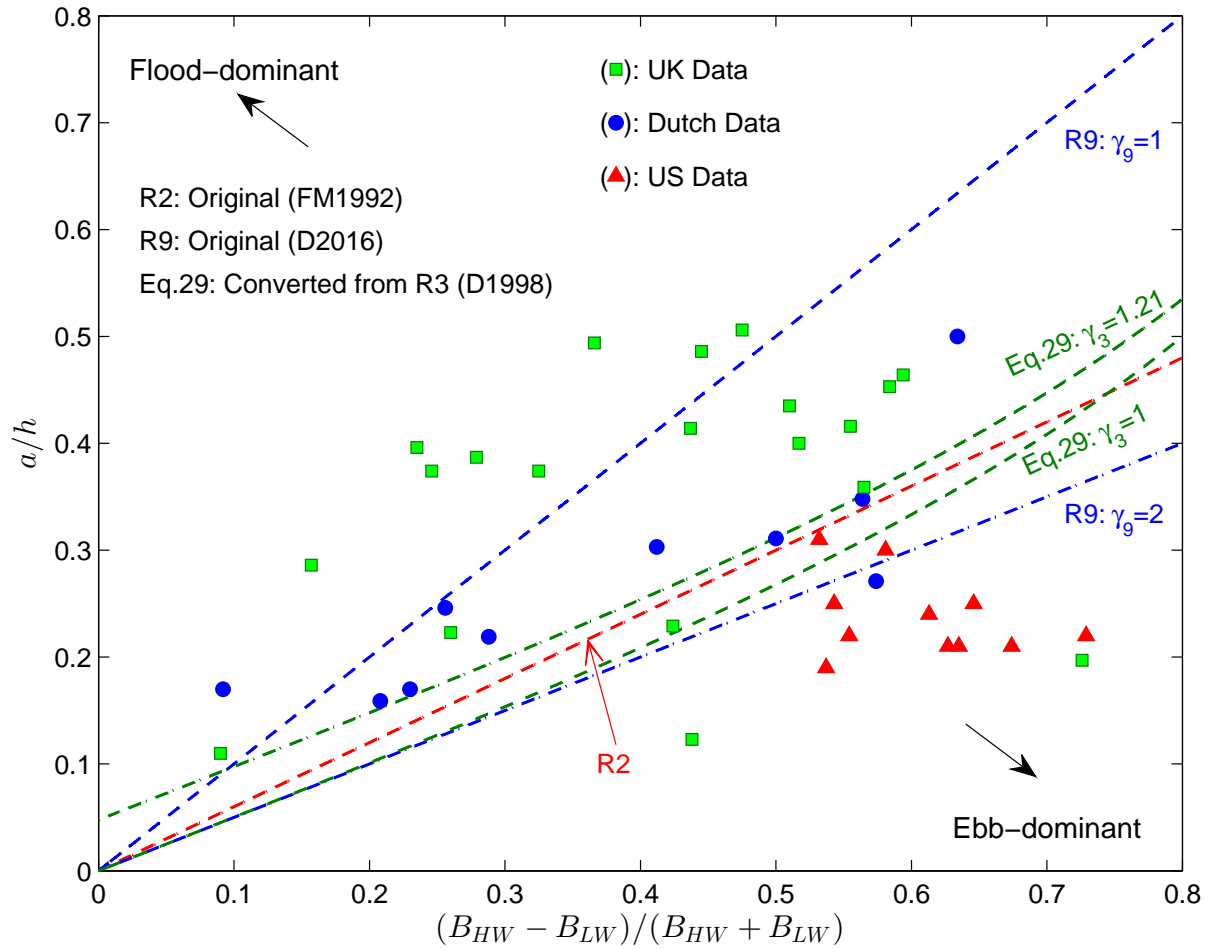


Figure 6: The existing and extended width-type relationships between $(B_{HW} - B_{LW})/(B_{HW} + B_{LW})$ and a/h as shown in Table 1 and derived in the main text. The points indicated by blue circles are the converted Dutch data from Dronkers (1998), red triangles are the converted US data from Friedrichs and Aubrey (1988) and green squares are the converted UK data from Townend (2005).

490 Dronkers (2016) compared the width-type relationship ‘R9’ with extensive datasets,
 491 ranging from short tidal lagoons to long convergent estuaries, which will be further dis-
 492 cussed in the next section. Here we focus on the comparison of existing and converted
 493 TA-based relationships, as well as their comparison with the three published datasets
 494 (Figure 6). Not surprisingly, all of these relationships cluster within a certain narrow
 495 region as shown in previous figures, indicating the consistency among the geometric
 496 transformations. The overall spatial distribution of curves and data points in this width-
 497 type plot are particularly similar to the area-type (S_{HW}/S_{LW}) plot shown in Figure 4,
 498 indicating the inherent consistency between Dronkers (1998) and Dronkers (2016).

499 Similarly, the horizontal axis, $(B_{HWW} - B_{LW}) / (B_{HWW} + B_{LW})$, physically represents
500 intertidal storage whose increase leads to a more ebb-dominated system. Using the
501 cluster of TA-based relationships (excluding the curve “R9: $\gamma_9=1$ ” as discussed before),
502 it is evident that the UK data points tend to distribute within the flood-dominated zone
503 while the US points in the ebb-dominated zone. The selected Dutch basins are mostly
504 close to the purported equilibrium, as also discussed before. As demonstrated by
505 Dronkers (2016), the TA condition for different tidal systems should be viewed as site
506 dependent i.e. as a function of offshore difference in duration of falling and rising tide,
507 channel convergence length and some other factors (see Equation 13). This will be
508 further elaborated in the Discussion section.

509 **4 Discussion**

510 Simple estuarine stability relationships, either theoretical or (semi-)empirical, are par-
511 ticularly welcome by coastal scientists and engineers because they are normally easy
512 to use and capable of providing a rapid assessment on the morphological condition
513 of the tidal system. The most well-known of these is probably the (semi-)empirical
514 relationship between tidal prism and cross-sectional area (hereafter shorted as “PA re-
515 lation”). While the traditional PA relation has been under continuous exploration and
516 widely adopted as an indicator of estuarine equilibrium (D’Alpaos et al., 2010; Zhou
517 et al., 2014a), the theoretically inferred TA-based relationships have been paid much
518 less attention.

519 We have reviewed the three types of TA-based relationship formulated using differ-
520 ent geometries. Comparison of these relationships suggests an inherent consistency
521 among them. The TA condition of tide-dominated landforms is chiefly governed by the
522 competition between two physical parameters: the relative intertidal water storage and
523 the relative tidal amplitude (Friedrichs and Aubrey, 1988; Wang et al., 1999; Dronkers,
524 2016). The former is reflected by the three types of geometric ratio (e.g. $\Delta B / B_0$,

525 $S_{HW}/S_{LW}, V_S/V_C$) which affect the efficiency of water exchange, and subsequently in-
526 fluence the duration of flood and ebb tide. The latter, reflected by a/h , plays a major
527 role in determining the contribution of bottom friction on tidal flow propagation. A larger
528 relative intertidal storage usually tends to slow down the flood tide, resulting in more
529 ebb-dominated characteristic; while a larger relative tidal amplitude tends to consider-
530 ably reduce the ebb velocity, favouring flood dominance.

531 Despite their simple form, the use of these TA-based relationships does not appear
532 to be simple, primarily because of (i) what can be measured in practice; (ii) the impli-
533 cations of the assumptions made in the derivations; and (iii) uncertainties in the data
534 and limitations in the current approaches to TA analysis. These issues may hinder the
535 TA-based relationships being appropriately used in practice. In this section, we discuss
536 these issues in detail and propose several future research directions.

537 **4.1 Geometries assumed in 1D models and measured in practice**

538 Based on the 1D tidal equations, the existing TA-based relationships are mostly derived
539 by assuming a prismatic estuary with simple regular cross-sections (Figure 2). How-
540 ever, natural estuaries normally converge landwards both in width and depth, and are
541 characterised by various irregular cross-sections (Figure 7). To make use of a 1D solu-
542 tion, the section that defines the conveyance (i.e. the flow-conveying section) is the key
543 to getting representative hydrodynamics. This leads to a focus on propagation speed
544 and hence the hydraulic radius or, for wide systems, hydraulic depth. Below, we will
545 first introduce the approaches of estimating the conveyance section and the hydraulic
546 depth from natural estuaries and then discuss their effects on TA-based relationships.

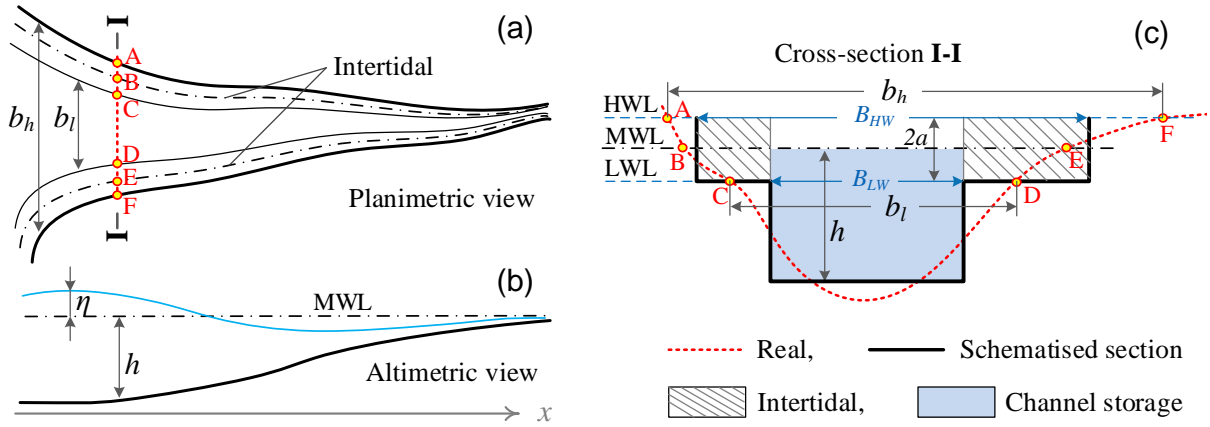


Figure 7: Sketch and geometrical parameters of an estuary. This figure is modified from Savenije (2012). Note that the measured widths at HWL and LWL (b_h and b_l) may be different from the ones of the schematised cross-section (B_{HW} and B_{LW}).

547 In practice, the geometric values of estuary width, surface area and volume are
 548 normally obtained at HWL and LWL (e.g. b_h and b_l in Figure 7a). These geometries
 549 can readily be extracted from charts, bathymetric surveys or satellite data. In addi-
 550 tion, the tidal range at the estuary mouth can be measured and is usually known to a
 551 reasonable degree of accuracy. The mean values of parameters used in the 1D tidal
 552 equations (e.g. the mean hydraulic depth h , the mean estuary channel width B_{LW} and
 553 the mean estuary top width B_{HW}) can be estimated using these measured quantities.
 554 For example, Dronkers (1998) proposed the following relationships:

$$h = a + \frac{V_{LW}}{S_{LW}} \quad (35a)$$

$$B_{HW} = \frac{S_{HW}}{L} \quad (35b)$$

$$B_{LW} = \frac{S_{LW}}{L} \quad (35c)$$

555 where, V_{LW} is the volume at LWL, and L is the length of the estuary. However, some
 556 studies also suggested different formulations for the mean hydraulic depth. Using the
 557 Stour and Orwell estuaries as study cases, Roberts et al. (1998) found the following
 558 relation of the mean hydraulic depth could be more reliable:

$$h' = \frac{1}{2}(h_{HW} + h_{LW}) = \frac{1}{2}\left(\frac{V_{HW}}{S_{HW}} + \frac{V_{LW}}{S_{LW}}\right) \quad (36)$$

559 where, h_{HW} and h_{LW} are the mean water depth at HWL and LWL, respectively, V_{HW}
 560 is the volume at HWL. Townend (2005) also defined the hydraulic depth using volume
 561 and surface area at the mean tidal level:

$$h'' = \frac{V_{MW}}{S_{MW}} \quad (37)$$

562 where, V_{MW} and S_{MW} are respectively the volume and the surface area at MWL.

563 Based on the measured data of the UK estuaries, the performance of the three
 564 different expressions of the mean hydraulic depth (h , h' , and h'') is compared against
 565 the volume-type TA relationships (Figure 8). Compared to the original Dronkers' ex-
 566 pression (h , Equation 35a), the other two approaches tend to result in assessments
 567 of tidal asymmetry that are even more flood-dominant. Noticeably, just a different way
 568 of estimating the mean hydraulic depth dramatically changes the a/h values, resulting
 569 in markedly different distribution of data points in Figure 8. This points to an inher-
 570 ent sensitivity in the method, making quantitative application difficult to interpret in any
 571 meaningful way.

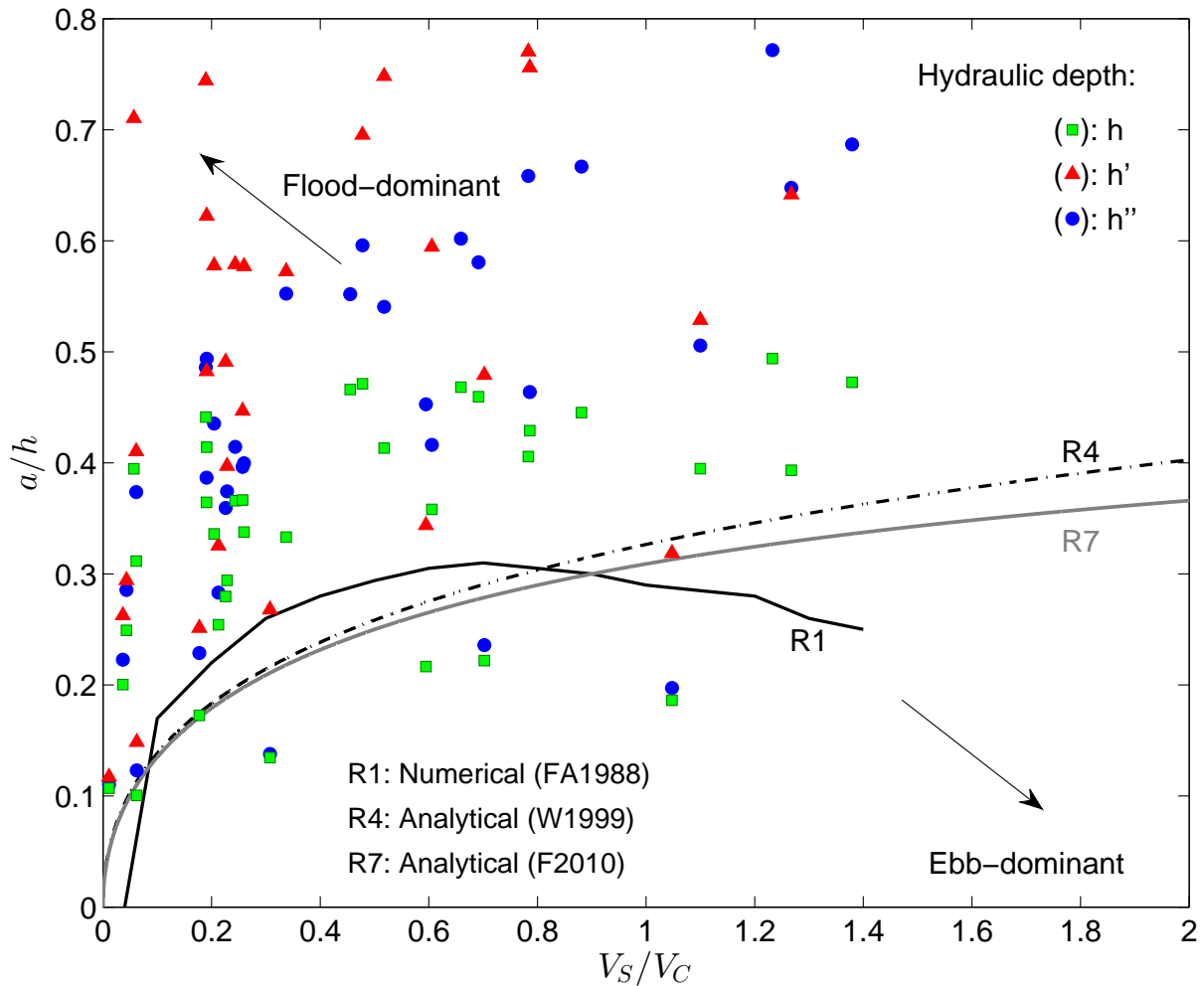


Figure 8: Different distributions of data points of a/h and V_S/V_C for different expressions of the mean hydraulic depth (h , h' , and h''), based on the UK estuary data of Townend (2005).

572 To facilitate the 1D model solution, a highly related quantity is the so-called con-
 573 veyance section. It is assumed, in most of the previous studies, that only the channel
 574 section (i.e. excluding intertidal area) is considered to be the flow-conveying part (Fig-
 575 ure 7c). The influence of this assumption can be seen in Figure 3 by comparing the
 576 curves R4 and R5 obtained respectively excluding and including intertidal area as the
 577 flow-conveying part. Compared to R4, the stability curve obtained with intertidal area
 578 included (R5) tends to shift to the ebb-dominant side. This essentially means that
 579 an estuary has more possibility to be categorised as a flood-dominant system using
 580 R5 (because intertidal area effectively enhances bottom friction, and tends to result in
 581 flood-dominant tidal flow). The rationality of excluding or including the intertidal area

582 as flow-conveying part, as well as its influence on the TA-based relationships, may be
583 readily examined using a 2D tidal model. In reality, the presence of a shallow sub-tidal
584 shoals can be found in many estuarine systems and this may also alter the effective
585 conveyance section.

586 Our analysis, therefore, suggests that these relationships may be of limited value
587 when used in isolation for management and conservation purposes. The key to ap-
588 propriately applying the TA-based relationships is to ground the analysis in a way that
589 ensures the celerity is correctly represented. Without some means of verifying the tidal
590 wave propagation, these TA-based relationships should be used with extreme caution
591 or not used to evaluate the condition of systems relative to equilibrium. In order to
592 ensure the correctness and representativeness of these estimated mean geometries
593 that are used in 1D models (and hence in TA-based relationships), it is vital to validate
594 the analytical (or simulated) tidal hydrodynamics against field measurements or more
595 sophisticated 2D numerical models. For example, contemporaneous data of water lev-
596 els, velocities, tidal phases at two or more locations along the estuary can be used to
597 estimate the celerity and hence confirm the geometric quantities such as the effective
598 conveyance section, the intertidal storage and the hydraulic depth (e.g. Friedrichs and
599 Aubrey, 1994; Cai et al., 2012; Savenije, 2012).

600 **4.2 Applicability of TA-based relationships**

601 Although these TA-based relationships display an overall consistency, it is still worth-
602 while to understand their physical background and hence applicability before choosing
603 a specific one, particularly because different assumptions were made for their deriva-
604 tion. For example, different schematic cross-sections were assumed and different sim-
605 plifications were made in the 1D tidal flow equations for analytical solutions. In fact, the
606 recent theory of Dronkers (2016) indicates that the TA-based relationship appears to be
607 site-dependent, because the TA index (γ_9) is a function of various site-specific parame-
608 ters (Equation 13). In particular, the offshore difference in duration of the flood and ebb

609 (Δt_{FR}^{mouth}) is one of the major factors affecting the behaviour of TA-based relationships.

610 Dronkers (2016) compared the width-type relationship R9 with data collected from
611 39 tidal landforms worldwide, including 18 tidal lagoons and 21 convergent estuaries
612 (Table A1). The comparison is shown in Figure 9. Noticeably, a large number of tidal
613 lagoons and estuaries tend to distribute around the curve indicated by “R9: $\gamma_9=2$ ”. Ac-
614 cording to Dronkers (2016), many of these tidal systems are close to equilibrium state.
615 Overall, the distribution of data points roughly indicates that tidal landforms with a larger
616 relative intertidal storage also have a larger relative tidal amplitude. In other words, the
617 linear width-type relationship R9 is generally in agreement with field data.

618 However, a number of estuaries are also found to locate far from the curves, clus-
619 tering within a narrow area defined by the value of $(B_{HW} - B_{LW})/(B_{HW} + B_{LW})$ being
620 smaller than 0.1. Dronkers (2016) did not include the data points of these systems
621 (i.e. indicated by grey markers in Figure 9) in his original plot because some of these
622 estuaries have a large fluvial discharge compared to tidal discharge, and hence the TA-
623 based relationships which assume a minor river influence do not hold anymore. Those
624 estuaries that distribute close to the curve “R9: $\gamma_9=2$ ” are found to have a small river
625 discharge compared to tidal discharge (e.g. WS, TH, DE, RI, DY and GO). Most of
626 these estuaries have a positive offshore tidal asymmetry with a shorter flood duration
627 ($\Delta t_{FR}^{mouth} > 0$), so their stability curves tend to move downward according to Equation
628 13, and hence the flood-dominant zone becomes larger in Figure 9. An exception is the
629 Humber estuary (HB) for which Dronkers found Δt_{FR}^{mouth} to be zero, hence its TA-based
630 stability relationship should have a relatively small γ_9 (i.e. the relationship should move
631 upward). The same holds for the French tidal lagoon Bassin Arcachon (BA) which even
632 has a negative Δt_{FR}^{mouth} . Typically, tidal systems with a wide continental shelf tend to
633 have a large and positive Δt_{FR}^{mouth} due to the distortion of tidal wave during propagation,
634 such as the Dutch basins. On the other hand, the interaction of the astronomical tides
635 may result in a negative Δt_{FR}^{mouth} in some tidal systems such as the US Willapa Bay
636 (WB). The reader is referred to Dronkers (2016) for more details.

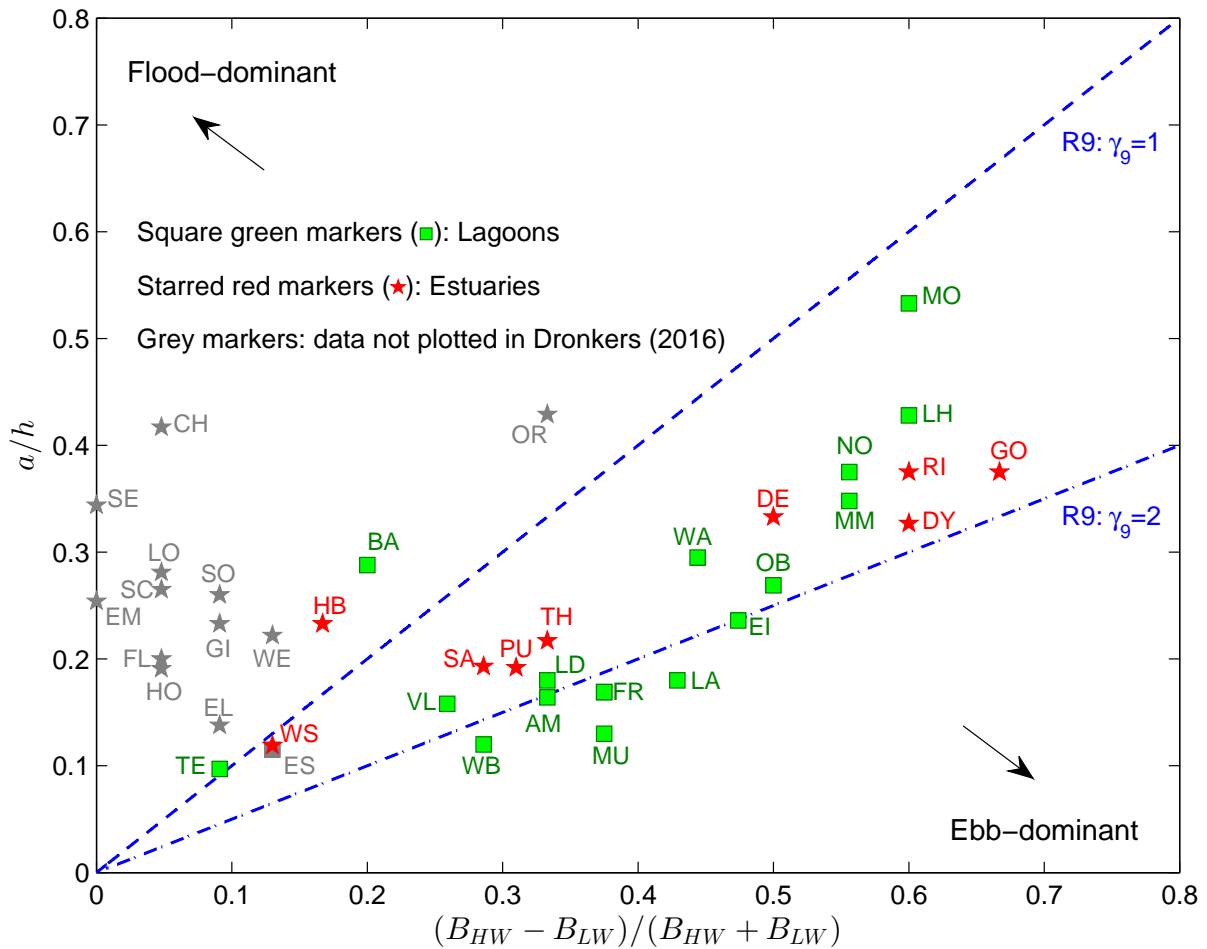


Figure 9: Comparison between datasets and width-type relationship R9 developed by Dronkers (2016). The data points indicated by stars indicate convergent estuaries, squares indicate short tidal lagoons. The grey markers indicate the data points that are not plotted in the original figure of Dronkers (2016), but shown in Table A1. The capital letters near the markers indicate specific tidal landforms of interest and discussed in the main text, refer to Table A1 for details. This figure is redrawn from Dronkers (2016).

637 Another point worth discussing is the influence of the planimetric estuary conver-
 638 gence which has been mostly neglected in existing studies. It is found that estuary
 639 convergence does not seem to play a significant role on the TA-based relationships, as
 640 also indicated by Friedrichs (2010). The 1D analytical solution of an exponentially con-
 641 vergent estuary proposed by Winterwerp and Wang (2013) can provide some insight.
 642 Following the work of Dronkers (2005) and Friedrichs (2010), they found that the TA
 643 index for convergent systems (γ_c) can be described by:

$$\gamma_c = \left[\frac{1 + a/h}{1 - a/h} \cdot \frac{\sqrt{(L_*^2 - (1 - a/h))^2 + \left(\frac{L_*^2 r_*}{1 - a/h}\right)^2} + (L_*^2 - (1 - a/h))}{\sqrt{(B_* L_*^2 - (1 + a/h))^2 + \left(\frac{B_* L_*^2 r_*}{1 + a/h}\right)^2} + (B_* L_*^2 - (1 + a/h))} \right]^{1/2} \quad (38)$$

644 where $L_* = 2\omega L_b / \sqrt{gh}$ is the dimensionless convergence coefficient, $r_* = r/\omega h$ is the
 645 dimensionless friction coefficient, and $B_* = B_{HW}/B_{LW}$. For friction-dominated systems
 646 (e.g. shallow tidal basins), Equation 38 can be simplified to:

$$\gamma_c \approx \frac{1 + a/h}{1 - a/h} \sqrt{\frac{1}{B_*}} = \frac{h + a}{h - a} \sqrt{\frac{B_{LW}}{B_{HW}}} \quad (39)$$

647 The above simplified equation does not include the convergence term anymore,
 648 so the effect of channel convergence on the performance of TA-based relationships
 649 is minor for shallow friction-dominated systems. One may notice that this simplified
 650 equation is consistent with Dronkers' theory and it shares a similar form as Equation
 651 (12) by assuming $B_{HW}/B_{LW} = S_{HW}/S_{LW}$. In fact, the derivation of these existing TA-
 652 based relationships has mostly considered the friction term as a major contributor in
 653 the momentum balance. Overall, it can be concluded that these TA-based relationships
 654 derived using prismatic channels should be equally applicable for shallow convergent
 655 systems such as tidal networks. However, owing to the spatially varying width of chan-
 656 nels (often in an allometric relationship with depth), the width-type TA relationships
 657 may not be the best choice for convergent systems. As an alternative, the area- and
 658 volume-type relationships can be considered. While for non-convergent systems, the
 659 width-type stability relationships are most convenient to apply since it is relatively easy
 660 to collect the width data.

4.3 Uncertainties, limitations and further research

There are also a few uncertainties that need to be noted when applying these TA-based relationships. To start with, the accuracy of the measured data for comparison or validation needs careful examination. Because of the limitations and uncertainties in the measuring approaches and techniques, the data collected in large-scale estuarine systems are usually not very accurate. For example, Townend (2005) found that the percentage differences between two studies in estimates of bulk properties of nine UK estuaries range from approximately 30% to 150%. The accuracy of data may bring uncertainties and difficulties in the interpretation of results when stability relationships are used. For example, the generality and applicability of the empirical PA relation which was originally fitted from the US observational data has been much debated (Gao and Collins, 1994; Townend, 2005; Zhou et al., 2014b). It is also noted that there are some inconsistencies in the Dutch data between Dronkers (1998) and Dronkers (2016). Apart from the reason that the data were measured in different years, it may also originate from different measuring approaches and techniques. In order to apply these stability relationships with more confidence, it is necessary to develop advanced data collecting and processing methodologies to ensure sound comparisons and validations. It may be worth noting that the more detailed swath and LiDAR datasets that are now becoming available may enable improved estimates of gross properties to be derived in the future. Another uncertainty is on the dominant processes that shape the morphology of tidal basins and estuaries. Different processes besides tidal currents may also play an important role in some tidal basins and estuaries. For example, using a combination of hydrodynamic measurements and sediment deposition records, Hunt et al. (2016) demonstrated that waves can be morphologically significant by influencing tidal and suspended sediment flux asymmetry (see also e.g. Green and Coco, 2014). Another commonly overlooked factor when formulating the TA-based relationships is the baroclinic effect that can alter the 3D flow structure, sediment settling and subsequently affect the morphological evolution of estuaries and tidal basins (Geyer

689 and MacCready, 2014; Gong et al., 2014). Therefore, the relative contribution of these
690 factors to shaping estuarine morphology compared to barotropic tides should be eval-
691 uated before the TA-based relationships can be used.

692 A final comment is made on the limitations of these TA-based relationships. First, a
693 number of assumptions were made to derive these relationships, including e.g. schematic
694 cross-sections and simplified 1D tidal equations. Hence, these relationships should not
695 be considered universally valid and their physical indications on natural systems should
696 be interpreted in a qualitative sense rather than a quantitative sense. For instance, the
697 theory of Dronkers (1998) is mostly applicable for relatively short tidal basins with a
698 symmetrical offshore tidal boundary and the approach of Friedrichs and Aubrey (1988)
699 and Friedrichs 1992 is for shallow friction-dominated systems. Second, the derivation
700 of these relationships is mainly based on the ratio between flood and ebb durations (or
701 the ratio between peak flood and ebb velocities) from purely a hydrodynamic perspec-
702 tive. However, the morphological indications are sometimes not so straight-forward.
703 This is an issue that is deeply embedded in the literature and reflects the dominance
704 of hydraulic approaches over morphological ones. For example, some UK estuaries
705 are found to export coarse sediment due to the ebb-dominated asymmetry in peak
706 velocities and import fine sediment due to flood-dominated asymmetry in slack water
707 durations. Third, TA is not the only factor determining the residual sediment trans-
708 port (and hence morphological change) while other factors such as river discharge and
709 compensation flow for Stokes drift can also play a role (Guo et al., 2014). Therefore,
710 the TA-based relationships should be applied with care, taking into account the many
711 influencing factors. Further research should be considered to (1) compare these TA-
712 based relationships with more accurate field datasets and 2D numerical models, (2)
713 relax some of the assumptions to develop more generic formulations, and (3) explore
714 the morphodynamic basis of equilibrium to develop an approach that more appropri-
715 ately defines system stability.

5 Conclusions

A synthesis of theories and formulations describing the relation between estuarine morphology and tidal asymmetry (TA) is provided in this study. Three different types of TA-based relationships, formulated using ratios of storage volumes, surface areas and basin widths, are discussed. These three geometric ratios are inter-converted to formulate additional stability relationships of the same metrics, so that different theories and approaches can be compared. The comparison indicates that most of these TA-based relationships tend to cluster within a narrow range, indicating the agreement among different theories. The relative intertidal storage reflected by the three types of geometric ratios (e.g. $\Delta B/B_0$, S_{HW}/S_{LW} , V_S/V_C), and the relative tidal amplitude reflected by a/h , are the two major controlling factors to determine the TA condition of a tide-dominated system.

Four published datasets are considered to compare with these different types of TA-based stability relationships. Against these data, a generally consistent indication of the TA condition is shown using different relationships, implying their inherent consistency. Depending on the data available, different relationships can be considered for practical use (e.g. estimation of a tidal system in response to short-term human interventions and long-term climate change). However, all the TA-based relationships are developed inevitably under various assumptions and their physical significance for natural systems should be interpreted with care. This is particularly the case when analysing a variety of tidal landforms with different types of hydrodynamic, sedimentologic and landscape settings.

The scatter exhibited by the various relationships is notably less significant than the scatter exhibited by the measured data. Given the expectation that most systems are responding to changes such as sea level rise and the nodal tide, suggests they are tracking some form of equilibrium, albeit with a lag (Wang and Townend, 2012). This leads to the conclusion that whilst these relationships provide some information about the tidal conditions, whether this provides a robust basis for determining morphological

744 stability remains an open question. Therefore, the use of these methods for manage-
745 ment and conservation points to a clear need. Whether they are fit for purpose is,
746 however, clearly questionable. There is therefore a need for research that explores the
747 morphological basis of equilibrium, to develop and, importantly, validate an approach
748 that more clearly identifies appropriate measures of system stability.

749 **Acknowledgements**

750 This study is supported by the Natural Science Foundation of Jiangsu Province (Grant
751 No. BK20160862), the National Natural Science Foundation of China (NSFC, Grant
752 Nos. 41606104, 51620105005), the National Key Research and Development Program
753 of China (Grant No. 2016YFC0401505) and the Fundamental Research Funds for the
754 Central Universities (Grant No. 2016B00714). We highly appreciate two anonymous
755 reviewers and the editors for their constructive comments. This is a ZORC contribution
756 1701.

Table A1: Geometric parameters of short tidal lagoons and convergent estuaries adapted from Dronkers (2016). Locations indexed by 1-18 are short tidal lagoons (L is the length of the flood basin), while the rest 19-39 are estuaries (L_b is the convergence length). The reader is referred to the main text for the meaning of parameters. The name of locations is indicated by two capital letters (shown in the column of Index/Identifier) which may be used in Figure 9.

Index/ Identifier	Data location	$\frac{a}{h}$	$\frac{B_{HW} - B_{LW}}{B_{HW} + B_{LW}}$	L or L_b (km)	$2a$ (m)	h (m)	Δt_{FR}^{mouth} (hour)
1-ES	Eastern Scheldt	0.115	0.130	40	3.0	13.0	0.1
2-TE	Texel Inlet	0.097	0.091	50	1.5	7.7	0.6
3-EI	Eijerland Inlet	0.236	0.474	12	1.7	3.6	0.5
4-VL	Vlie Inlet	0.158	0.259	25	1.9	6.0	0.4
5-AM	Ameland Inlet	0.164	0.333	22	2.1	6.4	0.6
6-FR	Frysian Inlet	0.169	0.375	20	2.3	6.8	0.2
7-LA	Lauwers Inlet	0.180	0.429	17	2.3	6.4	0.4
8-ED	Ems-Dollard	0.169	0.375	20	3.0	8.9	0.3
9-OB	Otzumer Balje	0.269	0.500	10	2.8	5.2	0.3
10-LD	Lister Dyb	0.180	0.333	20	1.8	5.0	1.2
11-LH	Langstone Harbour	0.428	0.600	5	3.25	3.8	-1.4
12-BA	Bassin Arcachon	0.288	0.200	15	3.0	5.2	-0.2
13-WA	Wachapreague	0.295	0.444	10	1.3	2.2	0
14-MM	Murrells Main Creek	0.348	0.556	7	1.6	2.3	1.0
15-MO	Murrells Oaks Creek	0.533	0.600	4	1.6	1.5	1.0
16-NO	North Inlet	0.375	0.556	6.5	1.5	2.0	0
17-WB	Willapa Bay	0.120	0.286	32	3.0	12.5	-0.6
18-MU	Mussolo Bay	0.130	0.375	26	1.2	4.6	0
19-WS	Western Scheldt	0.119	0.130	45	3.8	16	0.25
20-SC	Scheldt	0.265	0.048	21	5.3	10	0.75
21-TH	Thames	0.192	0.310	20	4.6	12	0.55
22-HB	Humber	0.233	0.167	30	5.6	12	0
23-DE	Dee	0.333	0.500	10	6.0	9	1.2
24-DY	Dyfi	0.327	0.600	6.5	3.6	5.5	1.5
25-RI	Ribble	0.375	0.600	6	6.0	8	0.6
26-EL	Elbe	0.138	0.091	40	3.3	12	0.9
27-WE	Weser	0.222	0.130	22	4.0	9	0.3
28-EM	Ems	0.254	0.000	22	3.3	6.5	0.6
29-SE	Seine	0.344	0.000	25	5.5	8	2.4
30-LO	Loire	0.281	0.048	23	4.5	8	1.6
31-CH	Charente	0.417	0.048	10	5.0	6	1.0
32-GI	Gironde	0.233	0.091	40	4.2	9	1.4
33-SA	Satilla R.	0.193	0.286	18	2.7	7	0.5
34-OR	Ord	0.429	0.333	15	6.0	7	0
35-HO	Hooghly	0.191	0.048	36	4.2	11	0.65
36-FL	Fly	0.200	0.048	40	4.0	10	0.1
37-SO	Soirap	0.260	0.091	22	2.6	5	0
38-GO	Gomso Bay	0.375	0.667	7.5	6.0	8	0.2
39-PU	Pungue	0.217	0.333	17	5.0	11.5	0.8

References

- 758
- 759 Aubrey, D. and Speer, P. (1985). A study of non-linear tidal propagation in shallow
760 inlet/estuarine systems Part I: Observations. *Estuarine, Coastal and Shelf Science*,
761 21(2):185–205, doi:10.1016/0272-7714(85)90096-4.
- 762 Boon, J. and Byrne, R. (1981). On basin hyposmetry and the morphodynamic re-
763 sponse of coastal inlet systems. *Mar. Geol.*, 40(1-2):27–48, doi:10.1016/0025-
764 3227(81)90041-4.
- 765 Brown, J. and Davies, A. (2010). Flood/ebb tidal asymmetry in a shallow sandy estuary
766 and the impact on net sand transport. *Geomorphology*, 114(3):431–439.
- 767 Cai, H., Savenije, H. H., and Toffolon, M. (2012). A new analytical framework for as-
768 sessing the effect of sea-level rise and dredging on tidal damping in estuaries. *Jour-
769 nal of Geophysical Research: Oceans*, 117(C9), doi:10.1029/2012JC008000.
- 770 D’Alpaos, A., Lanzoni, S., Marani, M., and Rinaldo, A. (2010). On the tidal prism–
771 channel area relations. *Journal of Geophysical Research: Earth Surface*, 115(F1),
772 doi:10.1029/2008JF001243.
- 773 Dastgheib, A., Roelvink, J., and Wang, Z. (2008). Long-term process-based morpho-
774 logical modeling of the Marsdiep Tidal Basin. *Marine Geology*, 256(1-4):90–100,
775 doi:10.1016/j.margeo.2008.10.003.
- 776 Davies, G. and Woodroffe, C. D. (2010). Tidal estuary width convergence: theory
777 and form in North Australian estuaries. *Earth Surface Processes & Landforms*,
778 35(7):737–749, doi:10.1002/esp.1864.
- 779 Dissanayake, D., Ranasinghe, R., and Roelvink, J. (2012). The morphological re-
780 sponse of large tidal inlet/basin systems to relative sea level rise. *Clim. Change*,
781 113(2):253–276.

- 782 Dronkers, J. (1986). Tidal asymmetry and estuarine morphology. *Netherlands Journal*
783 *of Sea Research*, 20(2-3):117–131.
- 784 Dronkers, J. (1998). Morphodynamics of the Dutch Delta. In Dronkers and (eds),
785 S., editors, *Proceedings of the 8th International Biennial Conference on Physics of*
786 *Estuaries and Coastal Seas.*, pages 297–304, Rotterdam: Balkema.
- 787 Dronkers, J. (2005). *Dynamics of coastal systems*, volume 25 of *Advanced series on*
788 *ocean engineering*. World Scientific, Singapore.
- 789 Dronkers, J. (2016). *Dynamics of coastal systems*, volume 41 of *Advanced series on*
790 *ocean engineering*. World Scientific, Singapore, 2nd edition.
- 791 Friedrichs, C. (2010). Barotropic tides in channelized estuaries. In Valle-Levinson, A.,
792 editor, *Contemporary issues in estuarine physics.*, pages 27–61. Cambridge Univer-
793 sity Press: Cambridge.
- 794 Friedrichs, C. and Aubrey, D. (1988). Non-linear tidal distortion in shallow well-mixed
795 estuaries: a synthesis. *Estuar. Coast. Shelf Sci.*, 27(5):521–545, doi:10.1016/0272-
796 7714(88)90082-0.
- 797 Friedrichs, C. T. and Aubrey, D. G. (1994). Tidal propagation in strongly convergent
798 channels. *J. Geophys. Res.*, 99:3321–3336.
- 799 Friedrichs, C. T., Aubrey, D. G., and Speer, P. (1990). Impacts of relative sea-level
800 rise on evolution of shallow estuaries. In Cheng, R. T., editor, *Residual currents and*
801 *long-term transport*, volume 38, pages 105–122. Springer, doi:10.1007/978-1-4613-
802 9061-9_9.
- 803 Friedrichs, C. T. and Madsen, O. S. (1992). Nonlinear diffusion of the tidal sig-
804 nal in frictionally dominated embayments. *J. Geophys. Res.*, 97(C4):5637–5650,
805 doi:10.1029/92JC00354.

- 806 Gao, S. and Collins, M. (1994). Tidal inlet equilibrium, in relation to cross-sectional area
807 and sediment transport patterns. *Estuarine, Coastal and Shelf Science*, 38(2):157–
808 172, doi:10.1006/ecss.1994.1010.
- 809 Geyer, W. R. and MacCready, P. (2014). The estuarine circulation. *Annual review of*
810 *fluid mechanics*, 46:175–197, doi:10.1146/annurev-fluid-010313-141302.
- 811 Gong, W., Jia, L., Shen, J., and Liu, J. T. (2014). Sediment transport in response to
812 changes in river discharge and tidal mixing in a funnel-shaped micro-tidal estuary.
813 *Continental Shelf Research*, 76(2):89107, doi:10.1016/j.csr.2014.01.006.
- 814 Green, M. O. and Coco, G. (2014). Review of wave-driven sediment resus-
815 pension and transport in estuaries. *Reviews of Geophysics*, 52(1):77–117,
816 doi:10.1002/2013RG000437.
- 817 Guo, L., van der Wegen, M., Roelvink, J. A., and He, Q. (2014). The role of river
818 flow and tidal asymmetry on 1-d estuarine morphodynamics. *Journal of Geophysical*
819 *Research: Earth Surface*, 119(11):2315–2334, doi:10.1002/2014JF003110.
- 820 Hunt, S., Bryan, K. R., Mullarney, J. C., and Pritchard, M. (2016). Observations of
821 asymmetry in contrasting wave- and tidally-dominated environments within a mesoti-
822 dal basin: implications for estuarine morphological evolution. *Earth Surface Pro-*
823 *cesses & Landforms*, 41(15):2207–2222, doi:10.1002/esp.3985.
- 824 Jarrett, J. (1976). Tidal prism - inlet area relationships. Technical report, US Army
825 Corps of Engineers, Waterway Experiment Station, Vicksburg, MS, USA.
- 826 Jewell, S. A., Walker, D. J., and Fortunato, A. B. (2012). Tidal asymmetry in a
827 coastal lagoon subject to a mixed tidal regime. *Geomorphology*, 138(1):171–180,
828 doi:10.1016/j.geomorph.2011.08.032.
- 829 Lanzoni, S. and Seminara, G. (2002). Long-term evolution and morphodynamic equi-
830 librium of tidal channels. *Journal of Geophysical Research*, 107(C1):3001–3001,
831 doi:10.1029/2000JC000468.

- 832 Nidzieko, N. J. (2010). Tidal asymmetry in estuaries with mixed semidiurnal/diurnal
833 tides. *J. Geophys. Res.*, 115(C8):C08006, doi:10.1029/2009JC005864.
- 834 Nidzieko, N. J. and Ralston, D. K. (2012). Tidal asymmetry and velocity skew over
835 tidal flats and shallow channels within a macrotidal river delta. *J. Geophys. Res.*,
836 117:C03001–C03001.
- 837 Parker, B. B. (1991). *TIDAL INTERACTIONS (REVIEW)*, chapter 13 The relative im-
838 portance of the various nonlinear mechanisms in a wide range of tidal interactions,
839 pages 237–268. John Wiley & Sons.
- 840 Ranasinghe, R. and Pattiaratchi, C. (2000). Tidal inlet velocity asymmetry in diurnal
841 regimes. *Cont. Shelf Res.*, 20(17):2347–2366.
- 842 Roberts, W., Dearnaley, M., Baugh, J., Spearman, J., and Allen, R. (1998). The sed-
843 iment regime of the stour and orwell estuaries. In J., D. and M.B.A.M., S., editors,
844 *Physics of Estuaries and Coastal Seas, Balkema, Rotterdam*, pages 93–102.
- 845 Savenije, H. (2012). *Salinity and Tides in Alluvial Estuaries*. 2nd completely revised
846 edition, www.salinityandtides.com edition.
- 847 Speer, P. and Aubrey, D. (1985). A study of non-linear tidal propagation in shallow
848 inlet/estuarine systems Part II: Theory. *Estuar. Coast. Shelf Sci.*, 21(2):207–224,
849 doi:10.1016/0272-7714(85)90097-6.
- 850 Toffolon, M. and Lanzoni, S. (2010). Morphological equilibrium of short channels
851 dissecting the tidal flats of coastal lagoons. *Journal of Geophysical Research*,
852 115(F4):F04036, doi:10.1029/2010JF001673.
- 853 Toffolon, M. and Savenije, H. (2011). Revisiting linearized one-dimensional tidal prop-
854 agation. *J. Geophys. Res.*, 116:C07007, doi:10.1029/2010JC006616.
- 855 Townend, I. (2005). An examination of empirical stability relationships for UK estuaries.
856 *J. Coast. Res.*, 21(5):1042–1053, doi:10.2112/03-0066R.1.

- 857 Townend, I. (2012). The estimation of estuary dimensions using a simplified form model
858 and the exogenous controls. *Earth Surface Processes and Landforms*, 37(15):1573–
859 1583, doi:10.1002/esp.3256.
- 860 van der Wegen, M. (2013). Numerical modeling of the impact of sea level rise on tidal
861 basin morphodynamics. *J. Geophys. Res. Earth Surf.*, 118, doi:10.1002/jgrf.20034.
- 862 van der Wegen, M. and Roelvink, J. A. (2008). Long-term morphodynamic evolution
863 of a tidal embayment using a two-dimensional, process-based model. *J. Geophys.*
864 *Res.*, 113:C03016, doi:10.1029/2006JC003983.
- 865 van der Wegen, M., Wang, Z. B., Savenije, H. H. G., and Roelvink, J. A. (2008). Long-
866 term morphodynamic evolution and energy dissipation in a coastal plain, tidal em-
867 bayment. *J. Geophys. Res.*, 113:F03001, doi:10.1029/2007JF000898.
- 868 van Maanen, B., Coco, G., and Bryan, K. (2011). A numerical model to simulate the
869 formation and subsequent evolution of tidal channel networks. *Australian Journal of*
870 *Civil Engineering*, 9(1):61–71.
- 871 van Maanen, B., Coco, G., and Bryan, K. (2013). Modelling the effects of tidal range
872 and initial bathymetry on the morphological evolution of tidal embayments. *Geomor-*
873 *phology*, doi:10.1016/j.geomorph.2013.02.023.
- 874 van Rijn, L. C. (2011). Analytical and numerical analysis of tides and salinities in
875 estuaries; part i: tidal wave propagation in convergent estuaries. *Ocean Dynamics*,
876 61(11):1719–1741, doi:10.1007/s10236-011-0453-0.
- 877 Wang, Z., Jeuken, C., and de Vriend, H. (1999). Tidal asymmetry and residual sedi-
878 ment transport in estuaries. Technical report, Delft Hydraulics (now Deltares), The
879 Netherlands.
- 880 Wang, Z., Jeuken, M., Gerritsen, H., De Vriend, H., and Kornman, B. (2002). Morphol-
881 ogy and asymmetry of the vertical tide in the Westerschelde estuary. *Cont. Shelf*
882 *Res.*, 22(17):2599–2609, doi:10.1016/S0278-4343(02)00134-6.

- 883 Wang, Z. B. and Townend, I. H. (2012). Influence of the nodal tide on
884 the morphological response of estuaries. *Marine Geology*, 291-294:73–82,
885 doi:10.1016/j.margeo.2011.11.007.
- 886 Whitehouse, R. J. S. (2006). Review and formalisation of geomorphological concepts
887 and approaches for estuaries. Joint Defra/EA Flood and Coastal Erosion Risk Man-
888 agement R&D Programme Report number: FD2116/TR2, Prepared by HR Walling-
889 ford, ABPmer and Prof Pethick. This report can be accessed freely via [www.estuary-
890 guide.net/pdfs/FD2116_TR2.pdf](http://www.estuary-guide.net/pdfs/FD2116_TR2.pdf).
- 891 Winterwerp, H. and Wang, Z. (2013). Man-induced regime shifts in small estuaries – i:
892 Theory. *Ocean Dynamics*, 63:1279–1292, doi:10.1007/s10236-013-0662-9.
- 893 Zhou, Z., Coco, G., Jiménez, M., Olabarrieta, M., van der Wegen, M., and Townend,
894 I. (2014a). Morphodynamics of river-influenced back-barrier tidal basins: The role
895 of landscape and hydrodynamic settings. *Water Resources Research*, 50(12):9514–
896 9535, doi:10.1002/2014WR015891.
- 897 Zhou, Z., Coco, G., Townend, I., Olabarrieta, M., van der Wegen, M., Gong,
898 Z., D’Alpaos, A., Gao, S., Jaffe, B., Gelfenbaum, G., He, Q., Wang, Y.,
899 Lanzoni, S., Wang, Z., Winterwerp, H., and Zhang, C. (2017). Is “Mor-
900 phodynamic Equilibrium” an oxymoron. *Earth-Science Reviews*, 165:257–267,
901 doi:10.1016/j.earscirev.2016.12.002.
- 902 Zhou, Z., Olabarrieta, M., Stefanon, L., D’Alpaos, A., Carniello, L., and Coco, G.
903 (2014b). A comparative study of physical and numerical modeling of tidal net-
904 work ontogeny. *Journal of Geophysical Research: Earth Surface*, 119(4):892–912,
905 doi:10.1002/2014JF003092.